

© Copyright 2005

Hansang Cho

Classification of Functional Brain Data for Multimedia Retrieval

Hansang Cho

A dissertation submitted in partial fulfillment
of the requirements for the degree of

Doctor of Philosophy

University of Washington

2005

Program Authorized to Offer Degree:

Department of Electrical Engineering

University of Washington

Graduate School

This is to certify that I have examined this copy of a doctoral dissertation by
Hansang Cho

And have found that it is complete and satisfactory in all respects,
and that any and all revisions required by the final
examining committee have been made.

Chair of Supervisory Committee:

Linda G. Shapiro

Reading Committee:

Linda G. Shapiro

David P. Corina

James F. Brinkley III

Date: _____

In presenting this dissertation in partial fulfillment of the requirements for the Doctoral degree at the University of Washington, I agree that the Library shall make its copies freely available for inspection. I further agree that extensive copying of the dissertation is allowable only for scholarly purposes, consistent with "fair use" as prescribed in the U.S. Copyright Law. Requests for copying or reproduction of this dissertation may be referred to Proquest Information and Learning, 300 North Zeeb Road, P.O. Box 1346, Ann Arbor, MI 48106-1346, to whom the author has granted "the right to reproduce and sell (a) copies of the manuscript in microform and/or (b) printed copies of the manuscript made from microform."

Signature_____

Date_____

University of Washington

Abstract

Classification of Functional Brain Data for Multimedia Retrieval

Hansang Cho

Chair of the Supervisory Committee:

Professor Linda G. Shapiro
Department of Electrical Engineering
and Department of Computer Science and Engineering

This study introduces new signal processing methods for extracting meaningful information from brain signals (functional magnetic resonance imaging and single unit recording) and proposes a content-based retrieval system for functional brain data. First, a new method that combines maximal overlapped discrete wavelet transforms (MODWT) and dynamic time warping (DTW) is presented as a solution for dynamically detecting the hemodynamic response from fMRI data. Second, a new method for neuron spike sorting is presented that uses the maximal overlap discrete wavelet transform and rotated principal component analysis. Third, a procedure to characterize firing patterns of neuron spikes from the human brain, in both the temporal domain and the frequency domain, is presented. The combination of multitaper spectral estimation and a polynomial curve-fitting method is employed to transform the firing patterns to the frequency domain. To generate temporal shapes, eight local maxima are smoothly connected by a cubic spline interpolation. A rotated principal component analysis is used to extract common firing patterns as templates from a training set of 4100 neuron spike signals. Dynamic time warping is then used to assign each neuron firing to the closest template without shift error. These techniques are utilized in the development of a content-based retrieval system for human brain data.

TABLE OF CONTENTS

	Page
List of Figures	iv
List of Tables	v
Chapter 1: Introduction	1
Chapter 2: Detection of fMRI Activations	4
2.1. Background	4
2.2. Methodology	6
2.3. Experiments and results	16
2.4. Discussion	20
Chapter 3: A New Method of Neuron Spike Sorting	21
3.1. Introduction	21
3.2. Methodology	23
3.3. Results	33
3.4. Discussion.....	38
Chapter 4: Characterizing Neuronal Firing Patterns in the Human Brain	41
4.1. Introduction	41
4.2. Data	42
4.3. Methodology	42
4.4. Results	48
4.5. Discussion.....	50
Chapter 5: Query System for Content-Based Retrieval of Brain Data	52
5.1. Common features for both single unit recording and fMRI data	52
5.2. Data	52

5.3. Query algorithm and graphical user interfaces.....	61
5.4. Discussion.....	86
Chapter 6: Conclusion	87
6.1. Future directions of research	87
Bibliography	89

LIST OF FIGURES

Figure Number	Page
1.1. Whole picture of the research.....	2
2.1. Functional MRI in action.....	4
2.2. A typical hemodynamic response	7
2.3. Various hemodynamic responses.....	7
2.4. One level of decomposition by MODWT	8
2.5. Details and approximation of MODWT	10
2.6. Noise reduction by MODWT	11
2.7. Normalized partial energy sequences	12
2.8. Illustration of the DTW algorithm.....	14
2.9. Examples of finding path and searching area.....	15
2.10. ROC Curve comparison	18
2.11. Various hemodynamic responses by MODWT-DTW	19
2.12. One example of results by visual stimuli	20
3.1. An example of an electrode on multiple neurons	22
3.2. Microelectrode recording.....	23
3.3. Multiresolutional analysis of neuron signals.....	25
3.4. Filtering by MODWT	26
3.5. Normalized partial energy sequences	27
3.6. Principal component removed reconstructed signal	27
3.7. Examples of the heights and widths of neuron spikes	28
3.8. Error caused by Euclidean metric.....	30
3.9. Histogram of heights for entire neuron spikes.....	32
3.10. Extraction of background noise from real neuron signal.....	34
3.11. Generation of background noise	34

3.12. The amplitude-width histogram of the simulated signal	35
3.13. Templates for neuron spikes extracted by RPCA	37
3.14. Matching the firing times for each neuron.....	38
3.15. Variance estimation on real data	39
3.16. Flow chart	40
3.17. Semi-automated user interface	40
4.1. Comparison of power spectral estimation	44
4.2. Frequency firing templates.....	46
4.3. Time firing templates	46
4.4. Power spectrum and curve fitting	48
4.5. Local maxima and curve fitting	49
4.6. Finding the closest template by DTW	50
5.1. Brain anatomical parcellation scheme	56
5.2. Data structure for the content-based retrieval system	60
5.3. A file structure.....	62
5.4. A diagram of search routes.....	63
5.5. A screen shot of the initial search route selection	63
5.6. Query route by patient information	64
5.7. Query route by basic patient information with microelectrode number	65
5.8. Query route by patient information with location of microelectrode.....	66
5.9. Query route by patient information with fMRI temporal features.....	68
5.10. Query route by patient information with fMRI spatial features	68
5.11. Selection of patient information	69
5.12. A screen shot for choosing a trial for further querying.....	70
5.13. A screen shot displaying a list of neuronal firings.....	70
5.14. A screen shot displaying time and frequency patterns.....	71
5.15. Query by trial protocols with temporal single unit recording features.....	73

5.16. Query by trial protocols with spatial single unit recording features	73
5.17. Query by trial protocols with temporal fMRI features.....	74
5.18. Query by trial protocols with spatial fMRI features	74
5.19. Query by trial protocols by both fMRI and single unit recordings	75
5.20. A screen shot of the initial screen of query by trial protocols	76
5.21. A screen shot to select a brain location	77
5.22. A screen shot to select activation level and delay of HR	77
5.23. A screenshot to display a list of fMRI results for a spetic query.....	78
5.24. A screenshot to display fMRI activation results.....	79
5.25. A screenshot to select firing rate and time patterns.....	80
5.26. A screenshot to show neuronal firing patterns	81
5.27. Query by firing pattern with temporal SUR features	82
5.28. Query by firing pattern with spatial SUR features	83
5.29. Query by fMRI activation.	83
5.30. Query by brain location shared by both fMRI and SUR	84
5.31. Query by information of SUR for fMRI features.....	85
5.32. Query by fMRI information with SUR brain location	85
 6.1. A diagram to show the relationship of each index and query idea.....	 88

LIST OF TABLES

Table Number	Page
3.1. Classification results of simulation	36
5.1. Index of basic patient information	53
5.2. Index of protocols for single unit recording and fMRI data	54
5.3. Index of trial tasks for single unit recording and fMRI data	55
5.4. Index of spatial features for single unit recording data	57
5.5. Index of temporal features for single unit recording.....	58
5.6. Index of spatial features for fMRI data	59
5.7. Index of temporal features for fMRI data.....	60

Chapter 1

INTRODUCTION

The human brain is surely the least understood and most complex organ in the body. The function of the brain, including the detailed aspects of thinking is not yet understood. However, relatively recent technologies such as functional magnetic resonance imaging (fMRI), positron emission tomography (PET), electroencephalogram (EEG), and single unit recordings (SUR) allow the brain to be studied in much more detail than previously possible. There are at least two kinds of needs to address. First, advanced technologies are needed to effectively detect human brain activities from signals with high noise caused by patient movement, displacement of an electrode, different morphology, and so forth. Second, the information from a variety of biomedical fields, such as radiology, neurosurgery, and cognitive science, must be integrated, since it is impossible for one individual to comprehend every characteristics of each brain signal. The development of an integrative view is arguably only one way to truly understand the brain. [1]

Among the technologies to detect the function of the human brain, fMRI is recently becoming most prominent due to its ability to efficiently produce temporal characteristics as well as spatial images of the whole brain. However, fMRI detects the brain activities in a large region, i.e. hexahedron with 5~25 mm side each, which makes it hard to pinpoint the small-scale features of the brain. On the other hand, the single unit recording that collects neuronal firings from a single neuron is very valuable for understanding the properties of the brain at the cellular level, but it represents only a tiny area. If these two methods could be efficiently integrated into a single query system, the characteristics of the brain could be analyzed and understood in both large and small scale.

A content-based retrieval system is proposed to incorporate the information from both fMRI data and single unit recordings. In the retrieval system, various features of the brain can be queried using spatial-temporal descriptions. Before integrating the signal from the fMRI and single unit recordings, some crucial preprocessing is required. First, the activations of the fMRI must be found in a high-noise environment. Second, the neuron signals on an electrode should be classified according to their original sources, since one probe usually collects spikes from two or more neurons. Figure 1.1 gives an overview of the proposed system.

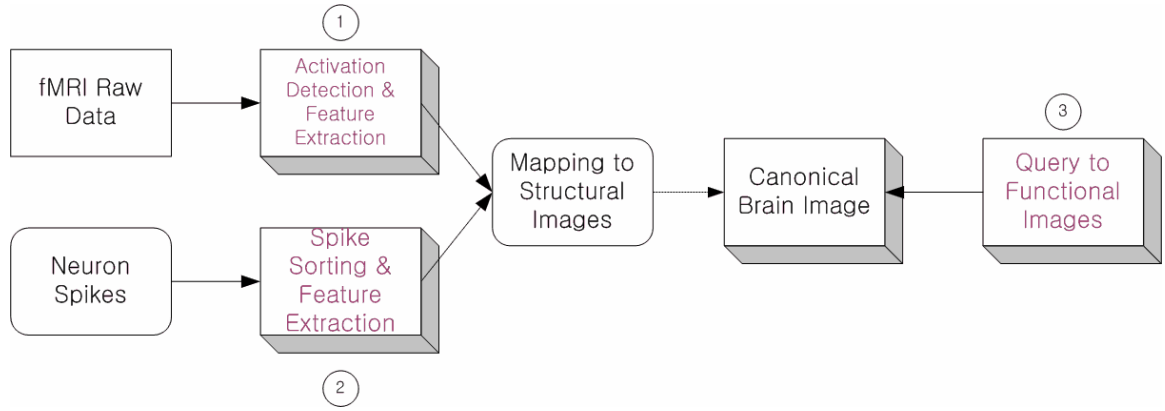


Figure 1.1 This block diagram shows the whole picture of this research. The circled numbers indicate the sequence. The activations of fMRI are transformed into canonical images, and then the neuron firing patterns are mapped onto them. Queries are performed on these canonical representations.

(1) We have developed a new method for dynamically detecting the activations of the fMRI that overcomes the weak points of the previous methods [2]. The maximal overlap wavelet transform is applied to the time-series signals of the fMRI to extract only the information related to the hemodynamic responses with minimum shape distortion. Then a dynamic time warping algorithm is utilized to classify the different types of waveforms.

(2) We have also developed new template-extracting method to discriminate the neuron spikes [3]. First, the neuron firings are filtered with a maximal overlap wavelet transform to obtain only the neuron-related signal. Then the rotated principal component analysis method is used to extract template shapes without the orthogonality limitation of the traditional PCA.

(3) A content-based retrieval system has been implemented for fMRI and single unit recordings. The fMRI activations and the single unit recordings are registered on a canonical brain image along with their indexes. Query algorithms for retrieval of fMRI and single unit recording data have been developed.

In Chapter 2, the method for detecting of fMRI activation will be shown. The spike sorting algorithm will be explained in Chapter 3, and the method for finding the characteristics of neuron firings will be described in Chapter 4. In section 5, the design of the content-based retrieval system will be described and examples of its uses will be given.

Chapter 2

DETECTION OF NEURAL ACTIVITY IN fMRI USING WAVELETS AND DYNAMIC TIME WARPING

2.1. Background

Functional magnetic resonance imaging (fMRI) is a noninvasive medical imaging tool to investigate physiological functions. Although fMRI can be applied to other organs, the current primary use of fMRI is to detect brain activity. As one performs a sensory, motor or cognitive task, specific brain regions increase metabolism. One of the outcomes of this activity is increased blood flow and subsequent changes in the ratio of deoxygenated and oxygenated hemoglobin. The differential paramagnetic properties of hemoglobin serve as a basis for the blood oxygenation level dependent (BOLD) MR contrast. Functional MRI allows researchers to study the function of the human brain by characterizing temporal and spatial properties of the BOLD signal.

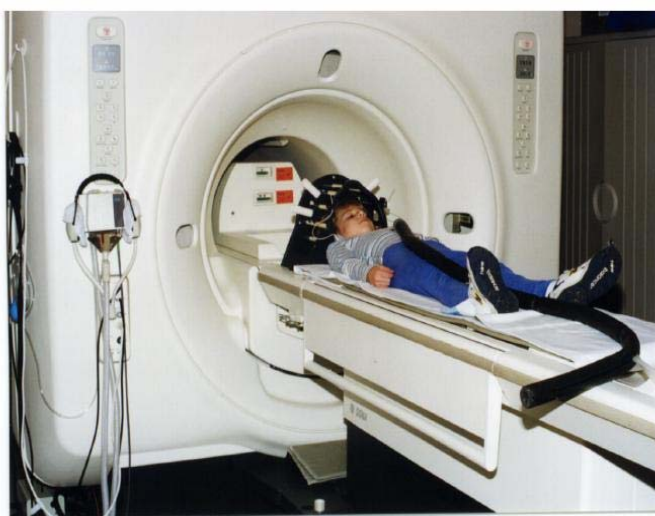


Figure 2.1. Functional MRI in action. The figure shows a patient prepared to enter a fMRI machine.

The typical fMRI experiment is a block design in which a subject is shown a stimulus and a cognitive task consisting of repetitive “on-off” patterns. For example, a subject is asked to name a picture during “on” status which lasts for several seconds, following “off” for more seconds. The “on-off” task, which is called a ‘boxcar’ design, repeats 5~10 times, and correlation or other statistical methods between the “on-off” reference signal and the signals from each of the voxels are used to detect activations. Recently event-related fMRI experiments have been used [4] [5] [6] in which the subject receives a brief stimulus in each epoch and the corresponding signals from voxels are measured. The event-related fMRI experiment has the advantage that it allows temporal measurement of brain activities, showing transient neural events [7] [8].

The detection of activations in the brain using event-related fMRI is difficult in that the hemodynamic responses in fMRI have relatively weak signals in which activations are only 0.5~5% of the average image intensity [9]. This problem can be solved with a repetitive experimental design in which the tasks are repeated several times and averaged in time; by this method, the noise is cancelled out. Furthermore, hemodynamic signals pose several quantification problems. First responses from different brain regions may vary from one another as a function of physiological properties and measurement errors. The commonly used hemodynamic impulse response is a difference between two Gamma functions which allows signal to have various delays and undershoots [10]. The typical hemodynamic response from the brain is given by

$$h(t, \tau_1, \tau_2, \delta_1, \delta_2, c_1, c_2) = c_1 \left(\frac{t-d}{\tau_1} \right)^{\delta_1} e^{-(\delta_1/\tau_1)(t-\tau_1)} - c_2 \left(\frac{t-d}{\tau_2} \right)^{\delta_2} e^{-(\delta_2/\tau_2)(t-\tau_2)} \quad (2.1)$$

where τ_1 and τ_2 determine the peak value and undershoot; δ_1 and δ_2 define the general shapes of the bumps, c_1 and c_2 determine the depth of undershoot

[Glover, 1999], and d represents the time delay of the hemodynamic response. These multiple changing parameters make it difficult to detect the fMRI activations with a reference signal that has fixed parameters. Therefore, a dynamic method is required to identify the various shapes of the output signals. The shape of a typical hemodynamic response is shown in Figure 2.2. Figure 2.3 shows different shapes of hemodynamic responses with various peak values, time delays, and overshoots.

The most popular method for detecting the activations in fMRI is a statistical approach, in which the boxcar in the block design or the reference hemodynamic response in the event-related design is considered as a hypothesis and a test statistic, such as the t-test, is applied. However, this statistical approach is very sensitive to noise, so the same events must be repeated several times. Another detection method is the direct measurement of activations using cross-correlation. The cross-correlation method may cause errors where there are time-shifts or slow responses, because it measures the correlation point by point. Furthermore, neither cross-correlation nor the statistical method is designed to detect various shapes [11] [12]. Other methods include independent component analysis (ICA), which is a blind source separation algorithm [13], principal component analysis (PCA) [14], and fuzzy C-Means clustering [15]. These methods do not require any prior knowledge about hemodynamic responses or experimental designs, but they are also unable to detect the various shapes of hemodynamic responses.

2.2 Methodology

Our analysis methodology was applied to signals that were rearranged in time series from the fMRI images. The white matter voxels in the 3-D fMRI images were aligned in the time domain, and a maximal overlap discrete wavelet

transform was then applied to each time series signal followed by a dynamic time warping method to detect the activations.

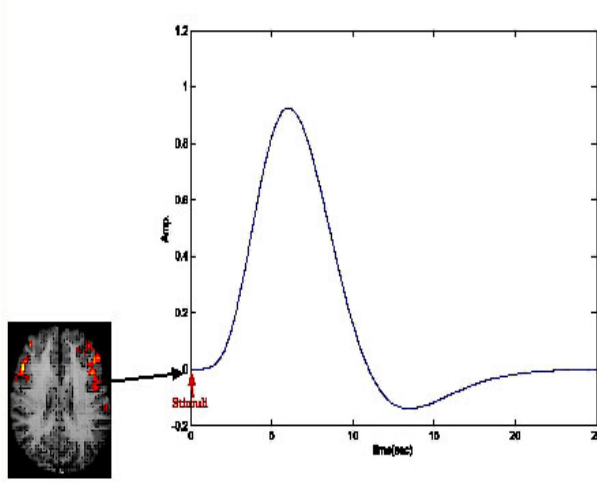


Figure 2.2. A typical hemodynamic response from the difference between two gamma functions.

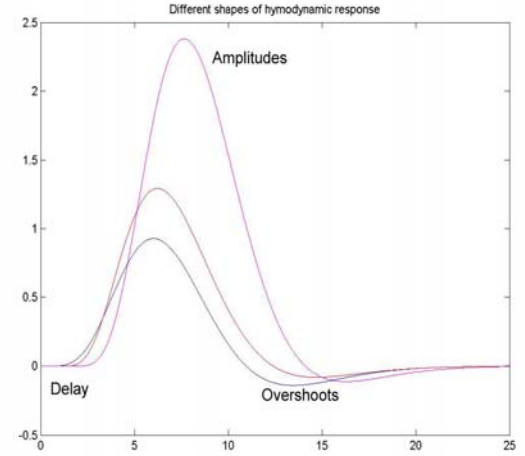


Figure 2.3. Various hemodynamic responses with different amplitudes, time-delay, diverse overshoots.

2.2.1 Maximal overlap discrete wavelet transformation

The wavelet method is one of the most popular ways to efficiently analyze signals in both the time domain and the frequency domain. The discrete wavelet transform, furthermore, is very useful in decomposing signals into a multi-resolution representation which consists of approximations and details. With the multi-resolution property, the diverse characteristics of the signal over various ranges from baseline change to variations of contiguous points are revealed. The multi-resolution characteristics cannot be shown in either the time-series signal or the frequency spectrum alone. The wavelet method to detect activated regions of the brain that correspond to a simple activation benefits from the fact that a smooth and spatially localized signal can be represented by a small set of localized wavelet coefficients, whereas the power spectrum of noise is uniformly spread throughout a wavelet transform space [16]. If the hemodynamic

responses can be extracted efficiently using wavelets, the repetition time to remove noise can be reduced.

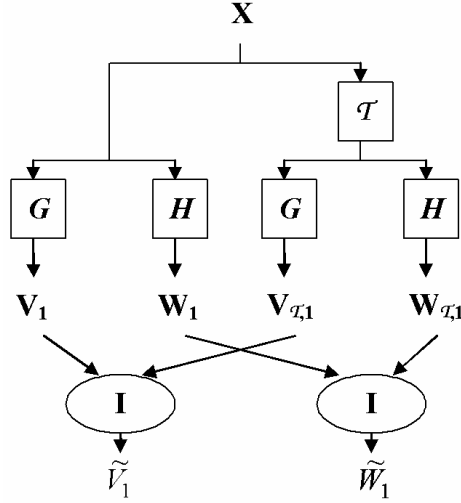


Figure 2.4. One level of decomposition by MODWT

Although the wavelet method has been previously used for detecting activations in event-related fMRI, it was only a kind of template matching using the Mexican hat wavelet as a template [Kobashi, 2001]. In our work, the maximal overlapped discrete wavelet transformation (MODWT) is used; by setting the coefficients of the finer detail levels in the spatial dimensions to zero and performing the inverse wavelet transform, a spatially smoothed version of data set can be reconstructed.

Since the MODWT has the characteristic that the time-shift of details and approximation of multiresolutional analysis are consistent with the time-shift of input signals [17], the MODWT is appropriate for the detection of fMRI activations. In contrast to the general discrete wavelet transform, the MODWT is not orthonormal and works for all sample sizes without requiring powers of two. To avoid the time shift of the wavelet transformation, the MODWT uses values downsampled from the discrete wavelet transform (DWT): The DWT pyramid

algorithm was applied twice, once to the original signal and once to the shifted signal, after which the two sets of DWT coefficients were merged.

The mathematical details of the MODWT are as follow. Let $\{h_l : l=0, \dots, L-1\}$ be real-valued wavelet filters with the width of the filter L and $H(\cdot)$ be the transfer function for $\{h_l\}$, i.e.,

$$H(f) = \sum_{l=-L}^L h_l e^{-j2\pi f l} \quad (2.2)$$

Let $g_l = (-1)^{l+1} h_{L-1-l}$ be scaling filters and G be the transfer function for $\{g_l\}$, i.e.,

$$G(f) = \sum_{l=-L}^L g_l e^{-j2\pi f l} = e^{-j2\pi f (L-1)} H\left(\frac{1}{2} - f\right) \quad (2.3)$$

Let \mathcal{T} be the circular shift matrix, which is given by

$$\mathcal{T} \bar{X} = [X_{N-1}, X_0, X_1, \dots, X_{N-3}, X_{N-2}]^T \quad (2.4)$$

Figure 2.4 shows one level of decomposition by MODWT, in which the original signal is applied to the DWT pyramid algorithm to generate the vector of the 1st level DWT scaling coefficients V_1 and the vector of the 1st level DWT wavelet coefficients W_1 . The DWT pyramid algorithm is then applied to the shifted signal $\mathcal{T} \bar{X}$ to get the shifted DWT scaling coefficients $V_{\tau,1}$ as well as the shifted DWT wavelet coefficients $W_{\tau,1}$. The wavelet coefficient \tilde{W}_1 is formed by rescaling the interleaved elements of W_1 and $W_{\tau,1}$, and \tilde{V}_1 is constructed in a similar way from V_1 and $V_{\tau,1}$.

The temporal input signal \bar{X} from each voxel in fMRI is deconstructed into details and approximation as following.

$$\bar{X} = \sum_{j=1}^{J_0} \tilde{D}_j + \tilde{S}_{J_0} \quad (2.5)$$

where \tilde{D}_j represents the MODWT details at level j and \tilde{S}_{J_0} is the approximation at level J_0 . Figure 2.5 shows the original input and the corresponding details and approximation. As seen in Figure 2.6, the low frequency baseline noise and the high frequency noise are eliminated successfully, which gives the temporal signal a clear shape.

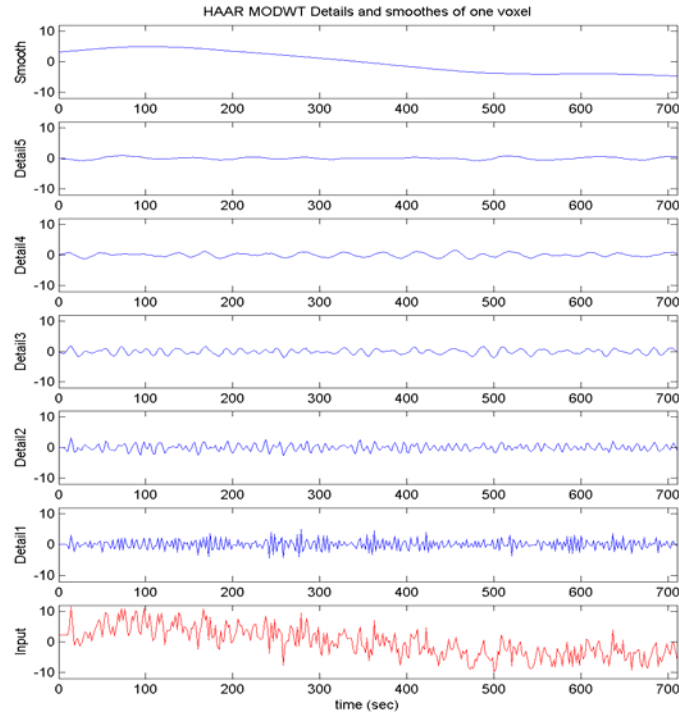


Figure 2.5 The details and approximation of MODWT. The bottom signal is the input signal from one voxel, the upper one is the approximation, and the rest are its details.

Although any wavelet basis may be used in this algorithm, the Haar wavelet is used as the wavelet transform kernel, because it is better at preserving the fine details and has the most compact spatial support of all wavelets [18]. To

verify the Haar wavelet's suitability for detecting activations in fMRI, a set of simulations were carried out. The simulation data consisted of 10 hemodynamic responses over 512 zeros points with adding uniform noise, Gaussian noise, and baseline. The Haar, the eighth order least asymmetric (LA8), and the eighth order Daubechies (D8) wavelet methods were applied to the simulation data. The normalized partial energy sequence (NPES) was used to evaluate these methods.

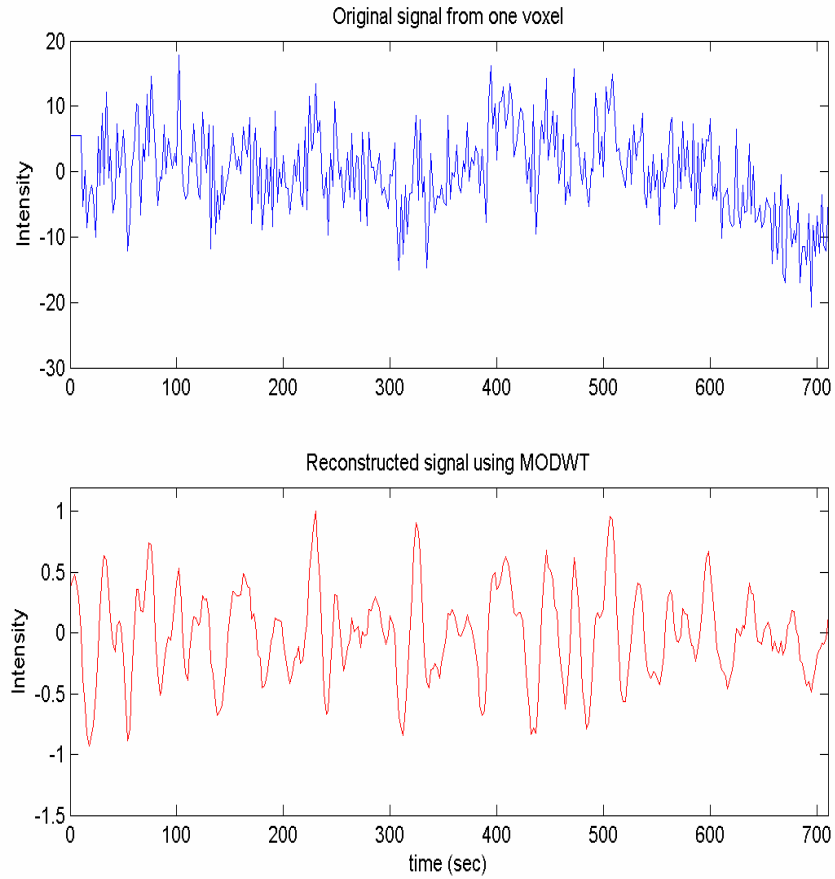


Figure 2.6 The upper one is the original signal from one voxel, and the bottom one is the reconstructed signal using MODWT. High frequency noise and baseline noise are removed.

For a sequence of variables $\{U_t : t = 0, \dots, M-1\}$, the NPES is defined as

$$C_n = \frac{\sum_{u=0}^n |U(u)|^2}{\sum_{u=0}^{M-1} |U(u)|^2}, \quad n = 0, 1, \dots, M-1 \quad (2.6)$$

where the $|U_{(u)}|^2$ represents the ordered squared magnitudes such that

$$|U_{(0)}|^2 \geq |U_{(1)}|^2 \geq \dots \geq |U_{(M-2)}|^2 \geq |U_{(M-1)}|^2 \quad (2.7)$$

If a particular transform can capture the key features in a time series with a few coefficients, the NPES C_n is expected to become close to unity for relatively small n [17]. As shown in Figure 2.7, the Haar method reaches unity earlier than the other tested methods, which makes it superior to the LA(8) or D(8) for summarizing the hemodynamic responses.

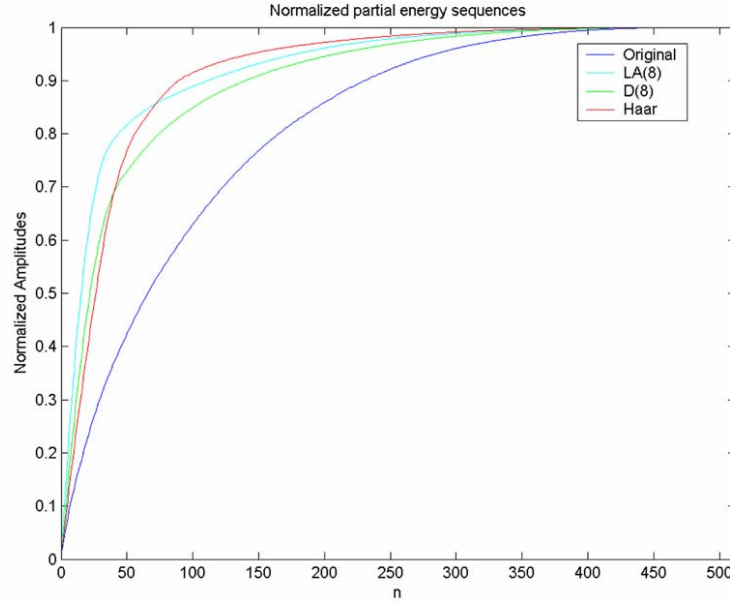


Figure 2.7 Normalized partial energy sequences of the LA(8), D(8), Haar(8), and the original neuron firing signal.

The temporal fMRI signals were decomposed into details and approximation by MODWT multiresolutional analysis. Some details were utilized for reconstructing the signal by the inverse MODWT, while other details and the approximation were set to zero to remove noise. Since the sampling rate is 2 seconds in our system and the hemodynamic response occurs at

approximately 20~25 second intervals, the third and fourth details keep their own signals in reconstruction. As seen in Figure 2.5, the sixth approximation contains the baseline noise, and the first and second details contain high-frequency background noise; both of these are removed by the construction.

2.2.2 Dynamic Time Warping

The method of dynamic time warping (DTW) is proposed as the second step for dynamically detecting the hemodynamic responses. DTW is well known in ultrasound imaging as well as in the speech recognition field. It is able to compensate for signal variability in a dynamic manner, finding the best possible warping of two time series: the reference signal and the hemodynamic responses from the brain [19]. Let $r(i)$, $i=1,2,\dots,I$ be the feature vector for the reference signal, and $q(j)$, $j=1,2,\dots,J$ be the vector for the hemodynamic responses. Let the reference $r(i)$ be placed at the abscissa and the responses from the brain placed at the ordinate on a two-dimensional grid. Representing this grid as a two-dimensional matrix d , the accumulated distortion measure D is defined by

$$D = \min_{\{M\}} \sum_{k=0}^{K-1} d(i_k, j_k) \cdot w(k) \quad (2.8)$$

where $d(i_k, j_k) = \|r(i_k) - q(j_k)\|_2$ is the distance between the respective elements of the strings $r(i)$ and $q(j)$, $M = \{(i_k, j_k), 1 \leq k \leq K\}$ is a search matrix with a reference signal in each row and a input signal in each column, k is the number of nodes along the path in the grid [20], and $w(k)$ is a nonnegative weighting coefficient, which is used intentionally to make D a more flexible measure. The optimal path procedure causes warping of the elements of the hemodynamic responses to the reference signal, resulting in the best matching. In other words, a smaller D means that the input signal is closer to the reference signal. To

determine the activated voxels in event-related fMRI, the cost function D should be smaller than the thresholds that are chosen by the user for each experiment. A smaller threshold makes the activation region more restrictive than a larger one. Figure 2.8 is an example for $I = 7$ and $J = 7$.

Although the DTW algorithm considers any minimum D to be a good solution, several constraints must be taken into account to get the best results. The first is the end-point constraint: the input signals have to go through the path

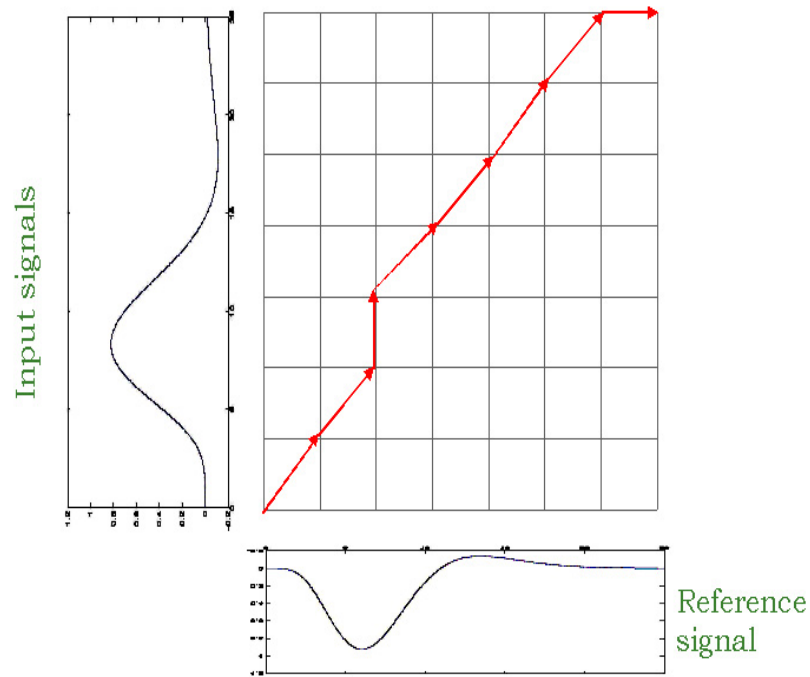


Figure 2.8 Illustration of the DTW algorithm that tries to find the optimal path

of the reference signal and must end at the same point as the test signal. The path is said to be complete if $(i_0, j_0) = (0, 0)$ and $(i_f, j_f) = (I, J)$. This means that the vector of hemodynamic responses should end at least near the end point of the reference vector, though it is not necessary for both end points to be identical. The second constraint is that only a one-step procedure is used to obtain the distance function $d(i, j)$, despite the fact that two or more steps may lead to a

shorter path, since the hemodynamic responses in fMRI would not fluctuate excessively [21]. So the cost d has the one-step form and the overall cost D is

$$D = \sum_{k=0}^{K-1} d(i_k, j_k | i_{k-1}, j_{k-1}) \cdot w(k) \quad (2.9)$$

Therefore, to be effective, global constraints for dynamic programming are applied in which the search subspace is the only region searched, since matrix elements outside of this space are considered to be inactive brain portions.

Since the hemodynamic responses used in this experiment have a sampling rate of 2 seconds and the amplitudes of the signals diminish after 22 seconds, the feature vector of the reference signal has 11 elements. However 12 elements of the brain signals to be measured were selected to optimize the capability to detect delayed responses. Each of the test vectors has the cost value D , after both the end point constraint and the global constraint are applied.

To use the dynamic-time-warping algorithm, the cost matrix is prepared by measuring the distances between each point of the reference signal and each point of an input signal. Starting from $(0,0)$ in this matrix, the optimal (i.e. shortest) path is found by following the minimum distance which produces the least cost. However, the optimal-path procedures cannot go backward in either x or y , which mean the next points from the current point at (i, j) can be only at $(i+1, j)$, $(i, j+1)$, or $(i+1, j+1)$, since the hemodynamic responses do not change abruptly. Furthermore, even though the cost is in a certain range, if the path lies outside the search subspace, this input is not considered as the desired hemodynamic response. Examples of path finding are shown in Figure 2.9.

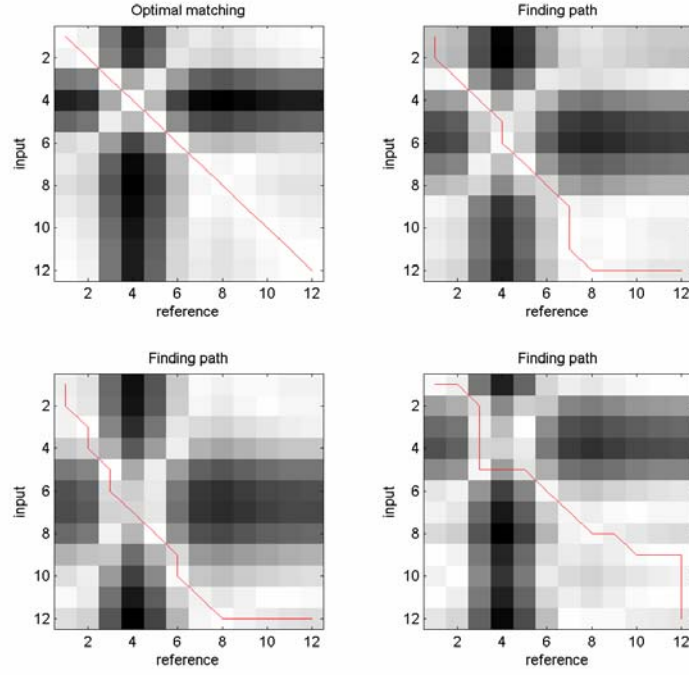


Figure 2.9 Examples of finding path and searching area. The upper left one has minimum distance.

2.3. Experiments and results

2.3.1 Simulation data

The MODWT-DTW method was evaluated using both simulated and experimental fMRI data. Since the activations in the human brain differ in subjects and experiment tasks, the simulated data had to be used to verify the method. For the simulation data, 500 signals that had acceptable hemodynamic responses and 500 randomly generated signals were used. The simulated hemodynamic responses are vectors with 12 element

$$\bar{Q} = \bar{H} + \bar{N} \quad (2.10)$$

where \bar{N} is a random vector of 12 elements with a Gaussian distribution $f_n = \frac{1}{2\pi} e^{-(x-1)^2/2}$. \bar{Q} is the feature vector sampled from the signal $q(t)$ with 2 second sampling rate from 0 second to 22 second:

$$q(t) = h(t) + n(t) \quad (2.11)$$

where $h(t)$ is the simulated impulse response of the hemodynamic signal in the form of equation (2.1) with different values of amplitudes, time-delays, and overshoots, and $n(t)$ is the noise with a Gaussian distribution.

The reference signal \bar{R} is the vector with 11 elements sampled from the signal $r(t)$, which has main amplitude $c_1 = 1$ and time delay $d = 0$, with 2 sec. sampling rate from 0 seconds to 22 seconds.

$$r(t) = \left(\frac{t}{5.4}\right)^6 e^{-1.11(t-5.4)} - (5.4) \left(\frac{t}{10.8}\right)^{12} e^{-1.11(t-10.8)} \quad (2.12)$$

In our experiments, the MODWT-DTW algorithm is applied to this \bar{Q} and \bar{R} .

The traditional method for analyzing the activation in fMRI is cross-correlation; it was also implemented in our experiments to compare the results with the MODWT-DTW. The cross-correlation is defined as

$$\bar{\rho}_{RQ} = \frac{1}{N} \sum_{i=1}^N Q_i R_i \quad (2.13)$$

where Q_i is the i -th element of the simulated vector for hemodynamic responses, and R_i is the i -th element of the reference vector. N is the number of elements; $N = 11$ in this experiment.

To access the performance of each method, receiver operating characteristics (ROC) curves were constructed. A ROC curve is a plot of the detection probability against the false alarm probability. For a given threshold, the detection probability is the fraction of all active voxels that are actually classified as active. In fMRI, a low false alarm probability is considered important; the ROC curve gives a hint of the fraction of active voxels that are not detected for a given fraction of false detection. Figure 2.10 shows the resulting ROC curves for MODWT-DTW and for cross-correlation from the simulated data set. It is evident that the MODWT-DTW method is much better than cross-correlation.

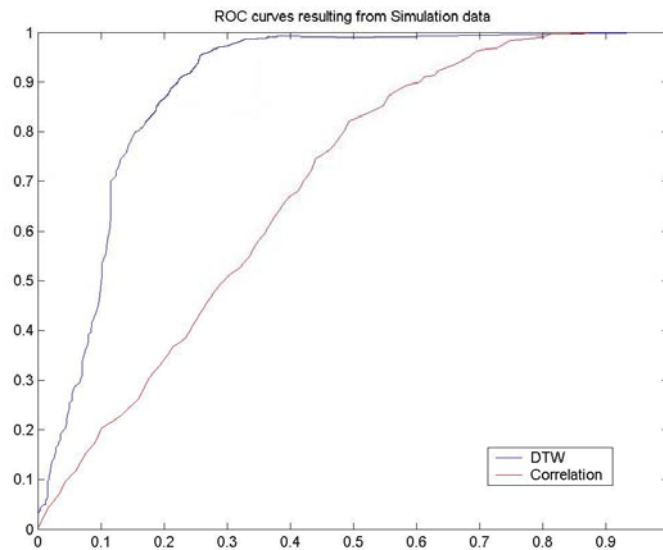


Figure 2.10 ROC Curve comparison between DTW and cross-correlation.

2.3.2 Real data

All fMRI images were acquired on a GE Sigma 1.5T system using a custom-built RF head coil, which increases the signal-to-noise ratio by 35% over the standard General Electric RF head coil. Structural images included sagittal (TR/TE 600/20ms) and axial (TR/TE 1/TE2 2000/35/80ms) views. The fMRI

acquisition used eight 7mm axial slices with a 1mm gap between slices (TR/TE 3000/40ms; 64x64 matrix; 90 flip angle; voxel size 7x3.75x3.75 mm) that covered 64mm of brain in the superior-inferior direction and centered on the sylvian fissure [22]. For this event-related experiment, both audio stimuli and visual stimuli were shown to the patients. To enhance the weak hemodynamic responses, the same events were repeated several times.

The brain images underwent several steps of preprocessing. First, image registration was performed to correct the error caused by the movement of the subject, which may cause unexpected detection; then a Gaussian smoothing filter was applied. After these procedures, the brain portions to be analyzed were obtained by image segmentation using the k-means algorithm. Only the time series from these segmented images, rearranged as vectors averaged over the repeated events, were used as the inputs for the dynamic time warping algorithm. After the analysis, the result vector was restored to the original brain area for display. Figure 2.11 shows the various shapes of hemodynamic responses detected by MODWT-DTW methods from our real fMRI data.

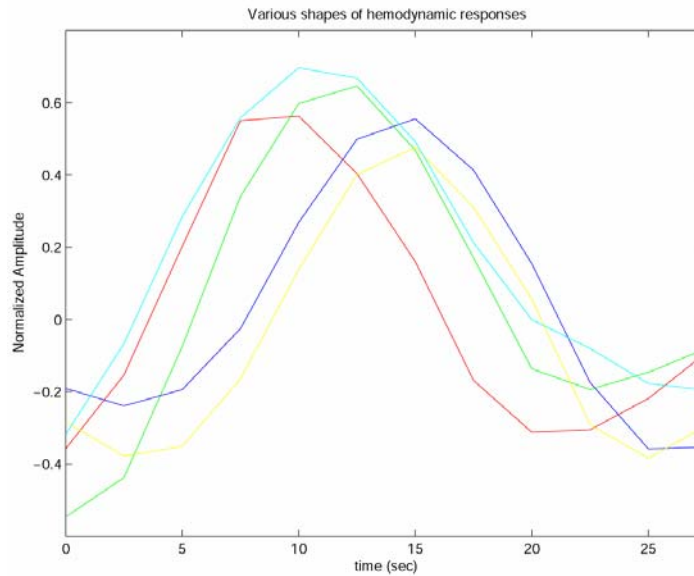


Figure 2.11 Various shapes of hemodynamic responses detected by the MODWT-DTW method

All preprocessing and fMRI data analysis by dynamic time warping for the simulated data set and real data set were implemented with Matlab 7.1 on Windows system. Figure 2.12 shows the results of the MODWT-DTW method. Colored voxels in the brain images indicate activated portions of the temporal lobe by the visual stimuli.

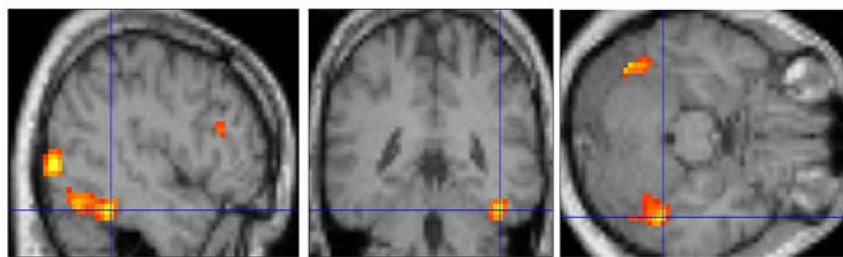


Figure 2.12: One example of results by visual stimuli. Colored voxels indicate activated portions of the fusiform region in the ventral portion of the temporal lobe. (a) sagittal plane (b) frontal plane (c) transverse plane

2.4. Discussion

The combined method of maximal overlap discrete wavelet transform followed by dynamic time warping to detect the activations in the fMRI is very effective at finding hemodynamic responses with different values of amplitudes, time-delays, and overshoots as well as low signal-to-noise ratio. In addition, the MODWT-DTW method can reduce the event repetition time.

The MODWT-DTW algorithm detects every activated voxel, even though only one voxel is valuable. Whether single voxel activation has any meaning or only large areas with consecutive voxels make sense is still arguable.

Chapter 3

SPIKE SORTING BY MAXIMAL OVERLAP DISCRETE WAVELET TRANSFORM AND ROTATED PRINCIPAL COMPONENT ANALYSIS

3.1. Introduction to spike sorting

Classification of neural spikes is a prerequisite for studying neural activity and brain functions. In extracellular recordings, an electrode placed in the cortex usually records spike activity from a number of neurons proximal to the electrode. Each individual neuron's signal, therefore, has to be separated by a classification method, which is called neuron spike sorting. The goal of spike sorting is to find the firing positions in time from each neuron. Background noise and baseline changes may make it difficult to separate the firings of one neuron from those of others. A stimulus results in the occurrence of a pattern of spike waveforms with different morphology and the possibility of overlapping activity. We present a new method that will remove background noise as well as the baseline to effectively extract accurate templates from the neuron signal itself. The desirable neuron template should hold common characteristics of the spike such as height and width, since the firings from a single neuron are believed to have same features.

A maximal overlap discrete wavelet transform is used for obtaining the specific bandwidth of the neuron signal, minimizing shape distortions that can be caused by a general band-pass filter. The original neuron signal, filtered by MODWT, is then segmented and the pieces are aligned according to amplitude. Next, a principal component analysis extracts the first principal component (PC) from these series of segments. The first PC is eliminated from each piece, and the segments are reconstructed into the original signal. Thereafter, the reconstructed signal without the first PC is aligned, and principal component analysis is run

again to extract the next principal component. This sequence is repeated until the variance is below a given threshold.

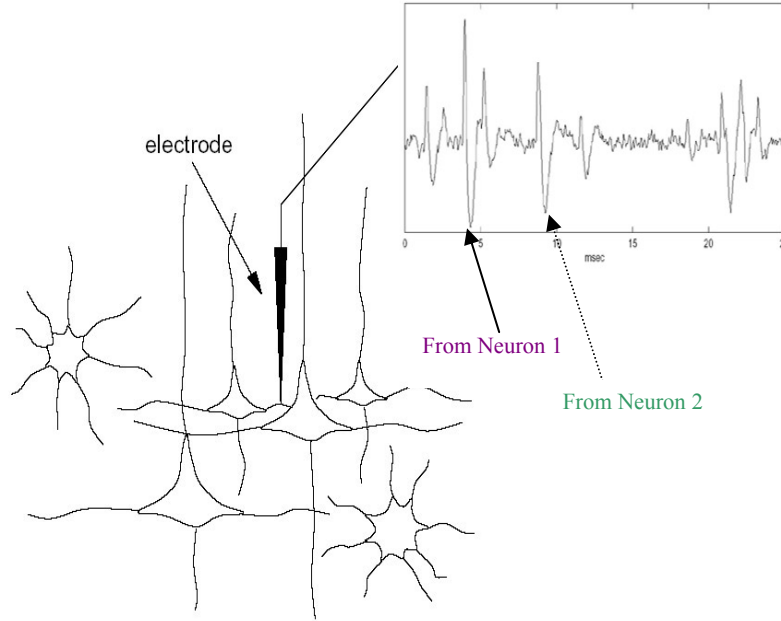


Figure 3.1. An example that an electrode can collect neuron firings from 2 neurons is showing.

A new template matching method for spike sorting based on shape distributions and a weighted Euclidean metric is proposed. The data is first roughly clustered using a Euclidean distance metric. Then the Levenberg-Marquardt method is used to estimate the variances of the neuron classes using curve fitting on the clustered data. Finally, the weighted Euclidean distance method is applied to minimize errors caused by different variances. This method provides optimized template matching results when the neuron variances are considerably different.

The sorted spike results are compared to a widely used method, the amplitude-width histogram approach, and utility of the method is demonstrated

through the use of this technique to identify temporal lobe neurons during language behavior in humans.

3.2. Method

Electrophysiological recordings were obtained during neurosurgery performed by Dr. George A. Ojemann in the Neurosurgery Department, University of Washington. For each patient, four extracellular electrodes were placed in the temporal lobe to collect neuronal firings. The microelectrode recording was performed in the sections of the cortex that were subsequently resected as part of the surgical therapy for epilepsy. Figure 3.2 shows the microelectrode recording process performed in the sections of the cortex that were subsequently resected as part of the surgical therapy for epilepsy.

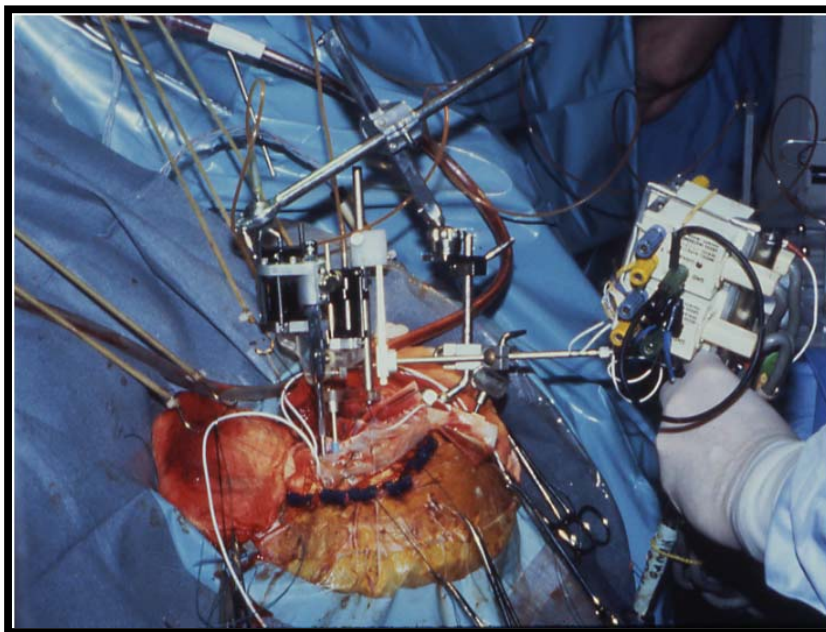


Figure 3.2. Microelectrode recording performed in the sections of the cortex that were subsequently resected as part of the surgical therapy for epilepsy.

3.2.1. De-noising

There are two kinds of noise found when sorting neuron spike signals: 1) jitter caused by amplification of the neuron signal and 2) baseline noise, such as 60Hz signals from electrical devices. Even though a general band-pass filter can remove both high and low frequency noise at the same time, it can cause shape distortion on spike signals, because an ideal filter cannot be implemented. Since the shapes of neuron firings are one of the most important factors in spike sorting, the general band-pass filter method may lead to large errors in spike classification. Taking this into consideration, the maximal overlapped discrete wavelet transformation (MODWT) is employed to extract the only bandwidth having information about the spike signal and to remove jitter and baseline noise. Since the goal of spike sorting is to find the positions of the firings in time for each neuron and since MODWT has the characteristic that the time-shift of details and approximation of multiresolutional analysis are consistent with the time-shift of input signals [17], the MODWT is appropriate for spike discrimination. The input neuron signal \bar{x} is decomposed into details and approximation as in (2.5). Figure 3.3 shows the original input and the corresponding details and approximation. As seen in Figure 3.4, the low frequency baseline noise and high frequency noise are successfully eliminated, which gives the firing signal a clear shape.

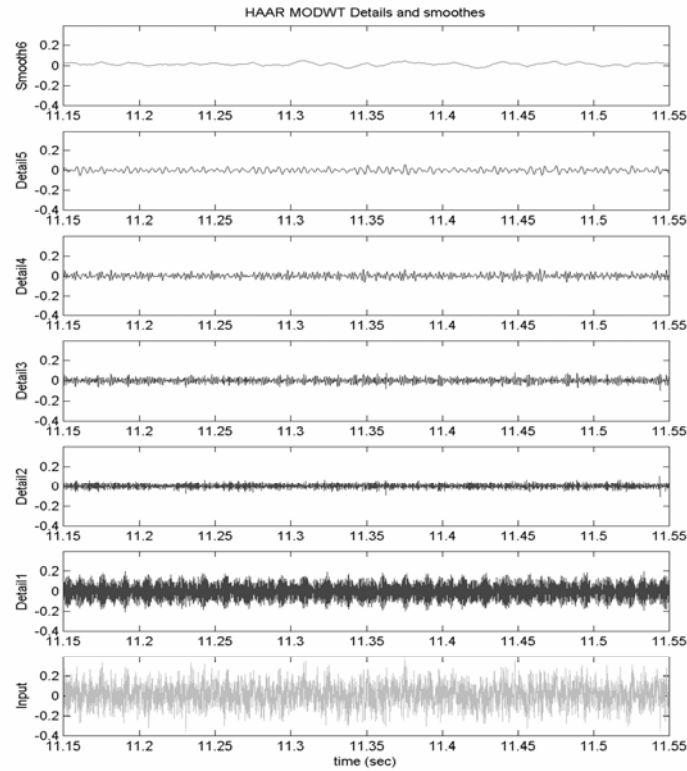


Figure 3.3 The bottom one is the input neuron signal, the figures in the middle are its details, and the top is its approximation which has baseline noise.

Although any wavelet basis may be used in this algorithm, the Haar wavelet is used as the wavelet transform kernel in the research, because it is better at preserving the fine details and has the most compact spatial support of all wavelets [18]. The normalized partial energy sequence (NPES), which was also used for the detection of activations in fMRI, demonstrates that the Haar MODWT is superior to other methods for neuron firing signals. As we can see in Figure 3.5, the Haar MODWT transform is able to represent the signal efficiently with fewer coefficients than the other methods.

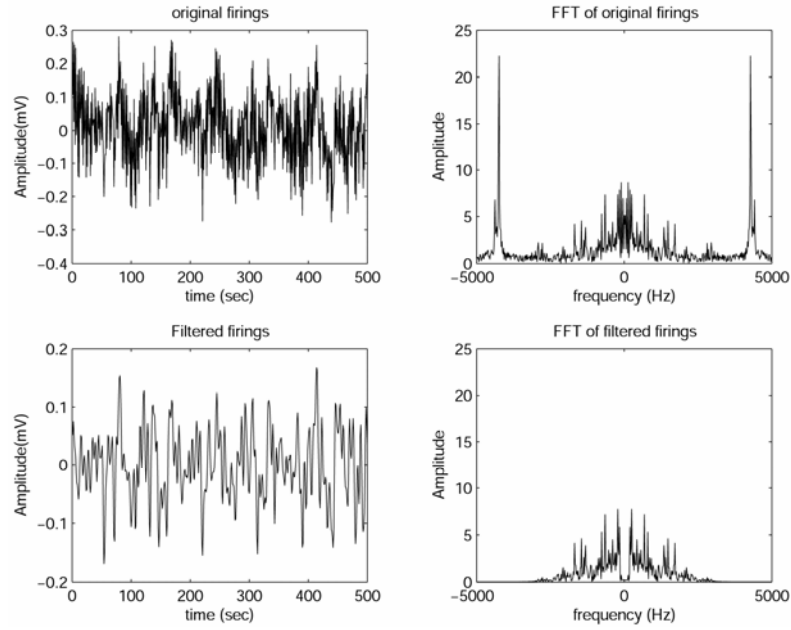


Figure 3.4. The top figures show the original neuron signal and its frequency component and the bottom figures show the filtered signal by MODWT and its frequency domain.

The neuron signal is decomposed into details and approximation by the MODWT multiresolutional analysis. Some of the details, which are only relevant to the neuron spikes, are utilized for reconstructing the signal by inverse MODWT, while the other details and approximation are set to zero to remove noise. The sampling frequency is 10 KHz in our system and the neuron firing occurs at approximately 3 millisecond intervals, which means that the information of a whole neuron is contained in around 30 points. The widths of the spikes, furthermore, are about 4~6 points. The 1st details of the MODWT have the information for 2 points, the 2nd ones are for about 4 points, the 3rd ones are for 8 points, and so on. So we need the 2nd through 5th details to comprehend the information of the neuron firings in about 4~32 points. Thus only the second through fifth details are kept in the reconstruction. As seen in Figure 3.3, the 6th approximation contains the baseline noise, and the 1st detail has high frequency background noise, both of which are removed when reconstructed.

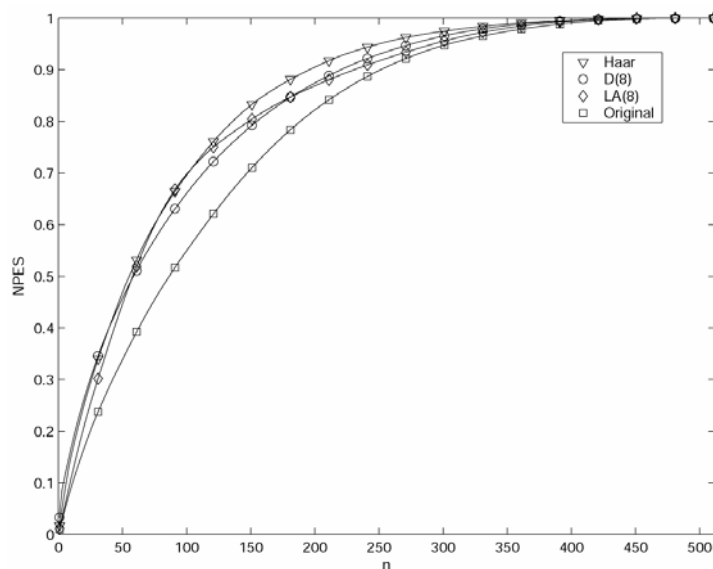


Figure 3.5. Normalized partial energy sequences of LA(8), D(8), Haar, and the original neuron firing signal.

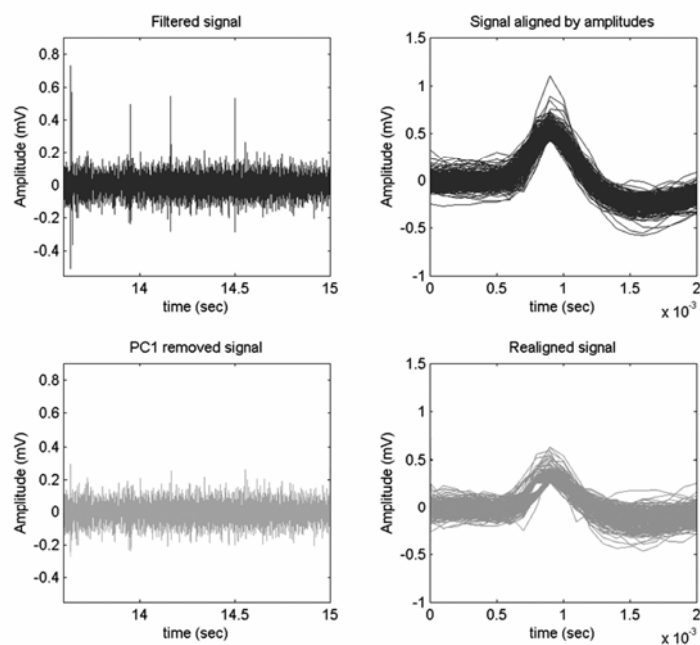


Figure 3.6. The top figures show the filtered signal and its alignment in amplitudes, and the bottom figures show the PC1-removed reconstructed signal and realignment.

3.2.2. Feature extraction

Principal component analysis (PCA) is a method that finds an ordered set of orthogonal basis vectors that capture the directions of largest variation in the data [23]. The PCA has been used in spike sorting to extract the neuron shapes [24], but this method has limitations due to its orthogonality property. In the traditional PCA methodology, neuron firings are aligned by amplitudes to determine the principal components. However, it is impossible for the second or third principal components to have proper neural shapes, because they are required to be orthogonal to the first principal component and the second principal component, respectively.

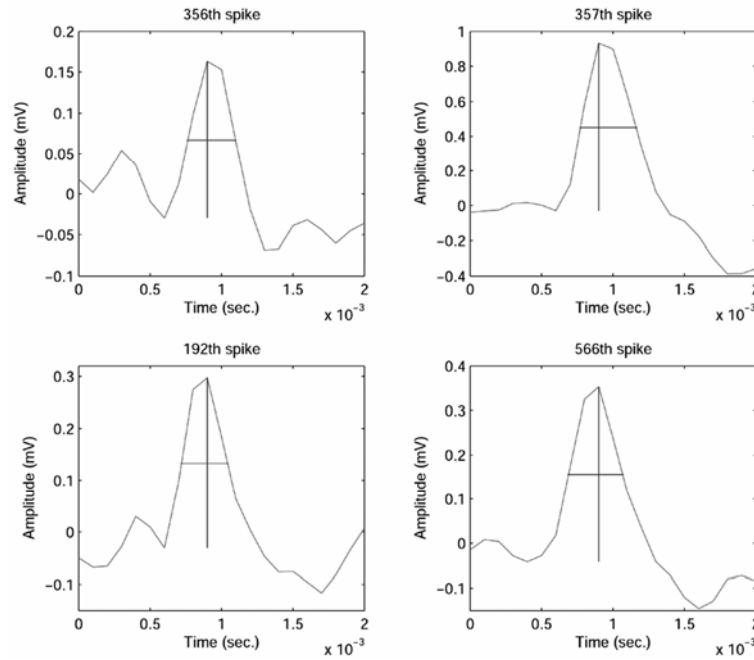


Figure 3.7 Examples of the heights and widths of neuron spikes

In this research, a rotated principal component analysis (RPCA) method is used to solve the problem. The first advantage of the RPCA is an ability to overcome the limitation of the orthogonality property of the traditional PCA. The RPCA has been employed in oceanology or meteorology to extract necessary

features excluding intrinsic characteristic like season variation [25]. For the neuron signal, the most prominent characteristic of the spike shape is its amplitude. The firings having heights above a threshold are aligned by amplitude, and traditional PCA is run to extract the first PC. The first principal component is then removed from the original neuron signal by

$$R_i(t) = X_i(t) - \bar{A} \cdot p(t) \quad (3.2)$$

where $R_i(t)$, $i = 1, 2, \dots, N$ is the sequence of the PC-removed segments, $X_i(t)$ is the previously aligned signal by amplitude, \bar{A} is the eigenvector of the PCA, and $p(t)$ is the principal component. The $R_i(t)$, $i = 1, 2, \dots, N$ are aligned with the original sequence at the previous time positions for reconstruction. The reconstructed signal is realigned by amplitudes so that PCA can again be applied to get the next PC. If the variance of the PCA is above the threshold, it means the principal component is dominant in the input segments. The step of PC extraction and reconstruction repeats until the variance is below the threshold, and then the principal components become templates for each type of neuron signal. The threshold for the dominant variance is determined by experiment. The other advantage of the RPCA is that it can discriminate the overlapped spikes efficiently, because the components of the most prominent template are removed from these overlapped firings and only the information from the other templates is left in the remaining signals.

Figure 3.8 shows the original filtered signal with its aligned segments on the top row, and the reconstructed signal with PC1 removed from each of segments and its aligned segments on the bottom row.

3.2.3. Classification by variance estimation

Due to the various shapes of neuron spikes and the lack of a priori knowledge about the neuronal information of each patient, the template matching method is a reliable method for spike sorting. After extracting templates, a Euclidean metric is used to calculate the distance to the templates, and then neuron spikes are clustered into nearest-neighbor classes.

A Euclidean metric is a very efficient way to classify data into nearest-neighbor templates when the classes have similar variances [23]. However, if the classes to be clustered have a wide range of variances, data in a class with larger variance can be misclassified into an adjacent class with smaller variance, resulting in errors. Fig. 3.8(a) demonstrates how a Euclidean metric can cause classification errors on neuron spikes having different variances. Provided that the class variances are already known, the classification errors can be decreased, as shown in Fig. 3.8(b). However, it is very difficult to measure variances for neuron clusters, since they differ for each neuron and the heights of neuron spikes are sometimes too close to separate.

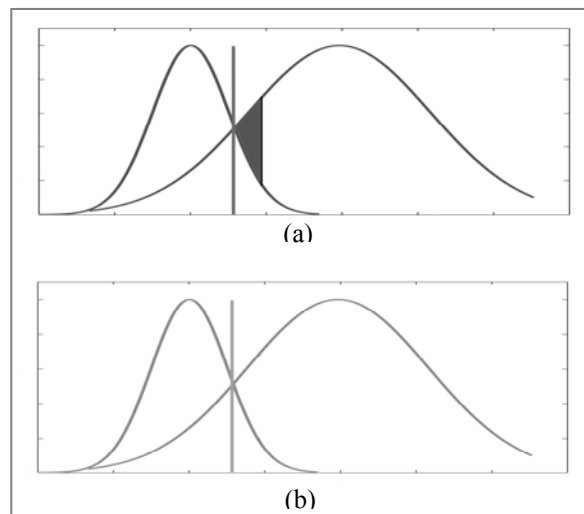


Fig. 3.8. a) Errors caused by applying a Euclidean metric to neuron classes with different variances; b) Improved classification using the known variances of the two classes

A new method for measuring variances of neuron firings using shape-based estimation, and for using the estimated variances to improve the classification process is proposed. The proposed method uses the Levenberg-Marquardt algorithm as a shape-based estimation method, in conjunction with a weighted Euclidean metric for refined template matching.

3.2.3.1. Variance Estimation

There is no a priori knowledge of the variances of neuron spikes, because each neuron has its own unique characteristics, such as mean values, variances, and firing patterns. Therefore, neuron spike variances have to be estimated using data dependent methods such as maximum likelihood estimation or the expectation maximization algorithm. However, previously classified data show that neuron spike classes are frequently too close to estimate variances using such statistical estimation methods. Fig. 3.9 shows the distribution of whole neuron spike heights, all from one patient, overlaid with the Gaussian distributions for each subclass. Since both the maximum likelihood estimation and expectation maximization algorithms try to find the proper number of Gaussian distributions, if the Gaussian mixture is too close, these methods do not effectively estimate variances.

To solve this problem, we propose a shape-based algorithm for estimating the variances of neuron spikes. Since the statistical estimation methods are not effective for estimating variances based on the data itself when the classes are too close, we assess variances based on the distribution shapes. Even though the variances of each cluster are extremely close, we can at least get partial shapes of the variances, which are then used to estimate the complete Gaussian shape

distributions. To acquire partial shapes of neuron spike classes, we apply a simple Euclidean distance method by which neuron firings are classified into nearest neighbor templates with minimum distances.

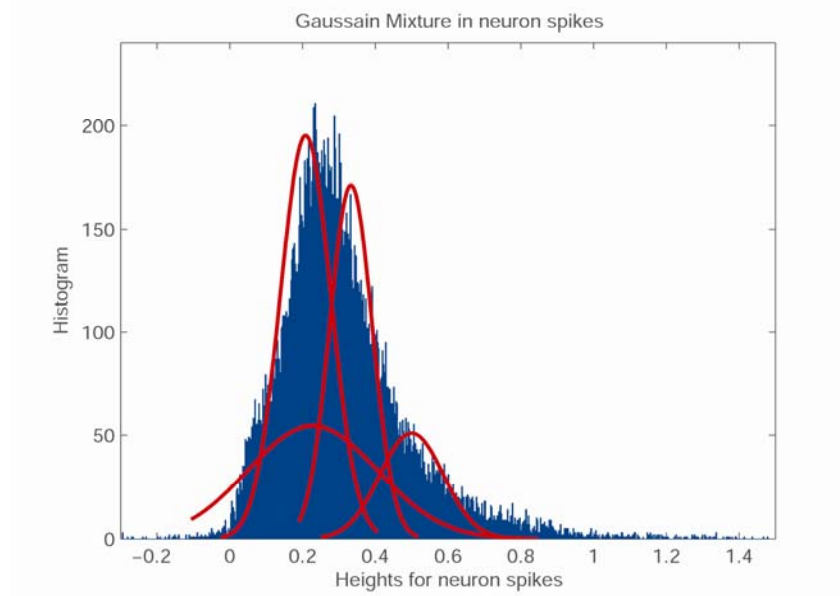


Figure 3.9. Histogram of heights for entire neuron spikes. Red lines represent Gaussian distributions for each class inside the whole histogram

To obtain the variances of each class, the heights of neuron spikes in a class are collected and the corresponding histograms are plotted. Furthermore, outliers, defined as points outside three times the standard deviation of the collected data, are removed to reduce distortion of the distribution shapes. The Levenberg-Marquardt method is used as a shape-based algorithm to estimate variances of neuron spikes. The Levenberg-Marquardt algorithm is for solving nonlinear least squares problems. It is a line search method whose search direction is a cross between the Gauss-Newton and steepest descent directions. The Levenberg-Marquardt finds the minimum of a function $G(x)$ that is a sum of squares of nonlinear functions:

$$G(x) = \frac{1}{2} \sum_{i=1}^m [g_i(x)]^2 \quad (3.3)$$

Let $J_i(x)$ be the Jacobian of $g_i(x)$; the Levenberg-Marquardt searches in the direction given by the solution p to the equations

$$(J_k^T J + \lambda_k I) p_k = -J_k^T g_k \quad (3.4)$$

where λ_k are nonnegative scalars and I is the identity matrix. [26] [27]. In this work, the curve fitting toolbox in Matlab were used for shape-based variance estimation.

3.2.3.2. Modified template matching

To obtain optimized classification results, a weighted Euclidean distance method is applied. The distance d_k between the input neuron spikes and templates is defined as

$$d_k^2 = \frac{\sum_k w_{ik} (x_{ik} - t_{ik})^2}{\sum_k w_{ik}} \quad (3.5)$$

where x_{ik} is the value of variable k in neuron spikes i , and w_k is a weight of 1 or 0, depending upon the inverse of standard deviations of neuron class k .

3.3. Results

3.3.1. Simulation data

A simulated neuron signal was used to verify the proposed method under known conditions. The simulated signal was designed with two spike templates from one actual neuron of a patient and background noise. The spike train lasted for 8 second duration (80,000 samples with 10 kHz sampling rate), embedded with 2000 neuron spikes from each template onto the background noise. The

background noise was extracted from a real neuron signal by setting zeros into the 2nd through the 5th details in the MODWT decomposition and applying the inverse MODWT. The signal associated with neuron spikes was removed, and only the noise part with baseline remained. Figure 3.10 shows the background noise extracted from an actual neuron firing and Figure 3.11 shows how to embed neuron spike templates into the background noise to make a simulation signal ready to be analyzed.

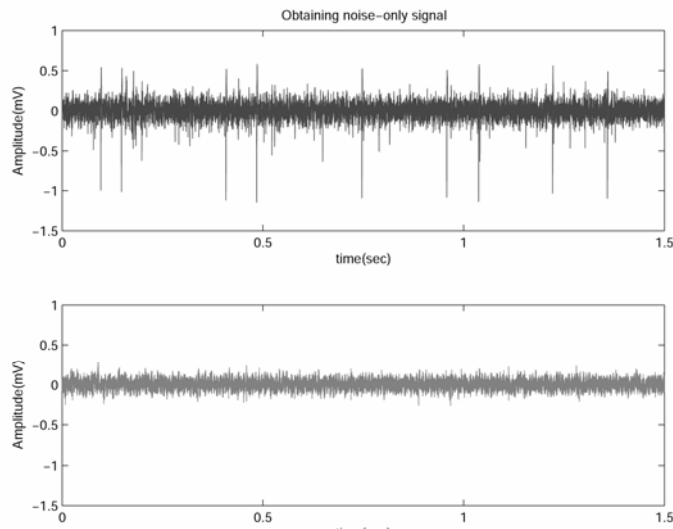


Figure 3.10. Extraction of background noise from real neuron signal. The upper one is the original neuron signal and the bottom one is the background noise.

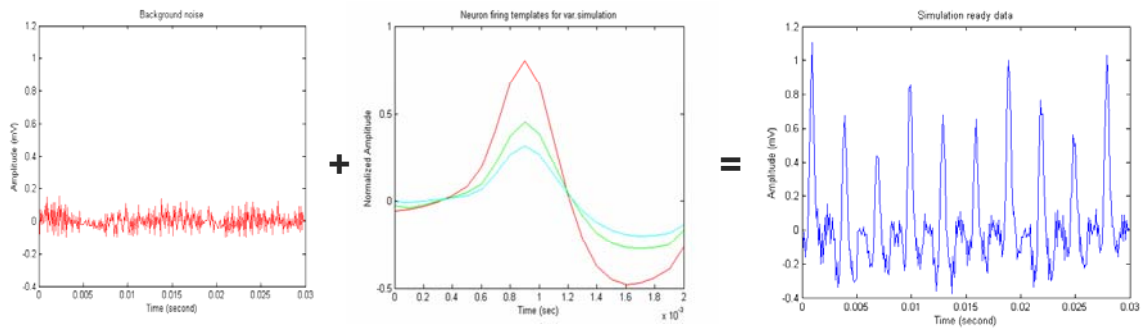


Figure 3.11. Three neuron spike templates (middle) embedded into background noise (left); simulation neuron signal ready to be analyzed (bottom).

The result of the MODWT-RPCA sorting method was compared with the amplitude-width histogram method [23] where the firings are scattered on a 2-D plane with amplitudes on the x-axis and widths on the y-axis. The histogram method is based on these scattered plots, and the spikes are discriminated by grouping the clusters by hand. As shown in Figure 3.12, the simulation data cannot easily be discriminated by the amplitude-width histogram due to the very close clusters. Using the MODWT-RPCA method, however, three sets of simulation data can be classified into 2 classes with 94.3%, 98.2%, and 96.2% respectively.

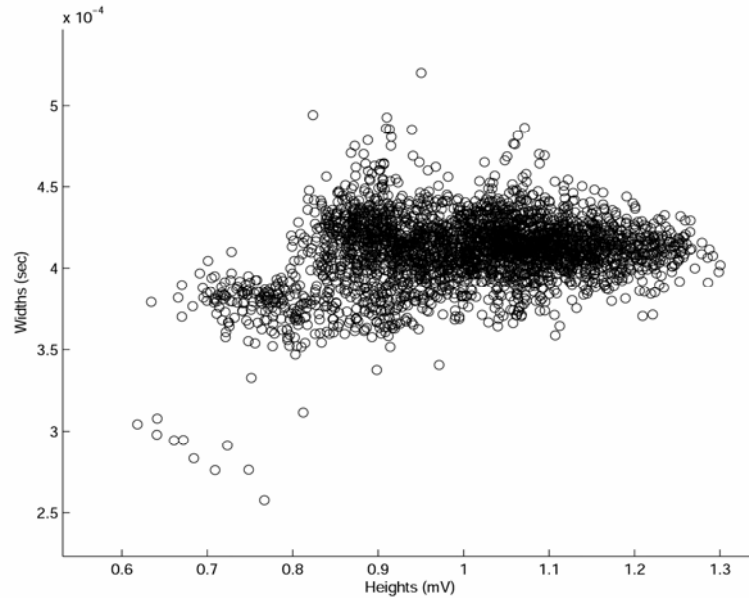


Figure 3.12. The amplitude-width histogram of the simulated signal. The widths and heights are too close to classify.

The new classification method, using the Levenberg-Marquardt algorithm and the weighted Euclidean distance, was applied to four kinds of simulation data with diverse variances. When the variances of three neuron spike classes are equal, the result obtained by our new method is the same as that obtained using the Euclidean distance alone. However, when the variances of three classes are significantly larger than the others, our method combining the Levenberg-

Marquardt algorithm and the weighted Euclidean distance improves classification efficiency. Table 5.1 shows a comparison of our new method with the Euclidean metric, in which the numbers represent accurate classifications out of 2000 neuron spikes per class.

3.3.2. Real data

The proposed method has also been applied to the neuron signals recorded from temporal lobes of human subjects. As we can see in the right column of Figure 3.4, the MODWT removes both higher and lower frequencies very efficiently, which makes the input neuron signal clear and minimizes shape distortion. Due to the effective filtering by MODWT, the templates for neuron spikes have coarse shapes that are closer to real spike firings. The left column of

	$\sigma_1 = 0.08, \sigma_2 = 0.08, \sigma_3 = 0.08$		$\sigma_1 = 0.12, \sigma_2 = 0.06, \sigma_3 = 0.06$	
	Euclidean	Weighted	Euclidean	Weighted
Neuron 1	1997	1998	1999	2008
Neuron 2	1989	1992	1826	1963
Neuron 3	2223	2219	2251	2105
	$\sigma_1 = 0.08, \sigma_2 = 0.12, \sigma_3 = 0.08$		$\sigma_1 = 0.07, \sigma_2 = 0.06, \sigma_3 = 0.12$	
	Euclidean	Weighted	Euclidean	Weighted
Neuron 1	1982	1992	1997	1997
Neuron 2	1726	2019	1201	1743
Neuron 3	2372	2009	2902	2360

Figure 3.13 shows examples of spike templates extracted from a signal on one electrode using RPCA. The classified results based on template matching are saved as files to represent firing times for each of the neurons.

TABLE 3.1: Classification results of simulation

The results were also compared with the amplitude-width histogram method. Though the amplitude-width histogram technique is not automated, nor is the measure of amplitudes or widths of firings precise, it may be used as a

reference because the results were checked, spike by spike, by experts. There was a reasonable matching between the proposed method and the amplitude-width histogram. For the comparison, neuron signals from two electrodes were applied to both methods. For the first electrode, both techniques found the same number of neurons, and two out of three neurons had meaningful neuronal behaviors. For the second electrode, the MODWT-RPCA was able to sort 2 neurons, one of which had neuronal meaning, while the amplitude-width histogram method did not discriminate neuron firing at all.

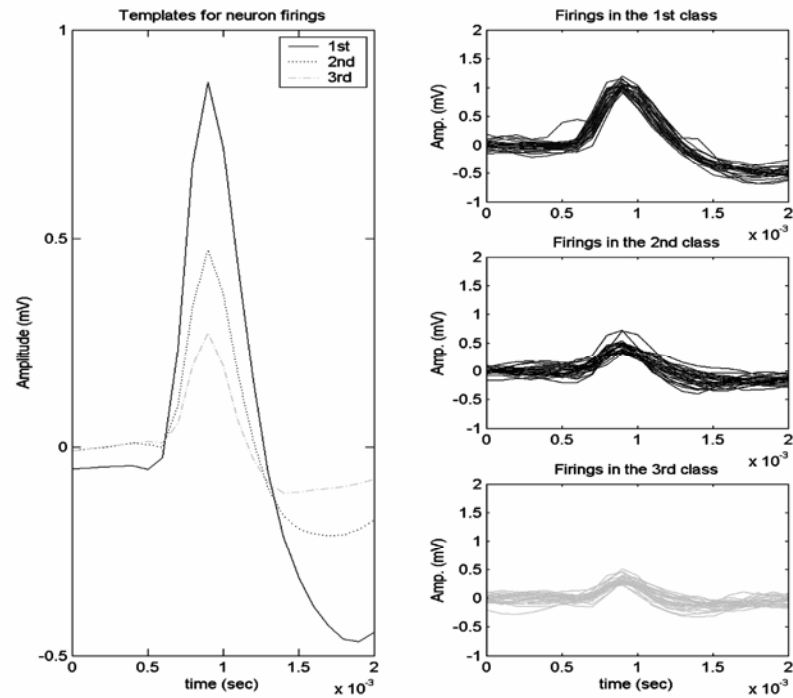


Figure 3.13. Templates for neuron spikes extracted by RPCA and spikes matched with the templates

Furthermore, the shapes of the firings were also verified by experts. The neuron firing sequences by the MODWT-RPCA method are consistent with a priori knowledge of neurological activities. The MODWT-RPCA spike sorting algorithm has proven to be excellent especially in high noise environments.

The shapes of real spikes classified to each neuron are shown in the right column in Figure 3.13; these were verified as valid neuron firings by experts in neurology. The firing time plots of classified spikes for each neuron are shown in Figure 3.14.

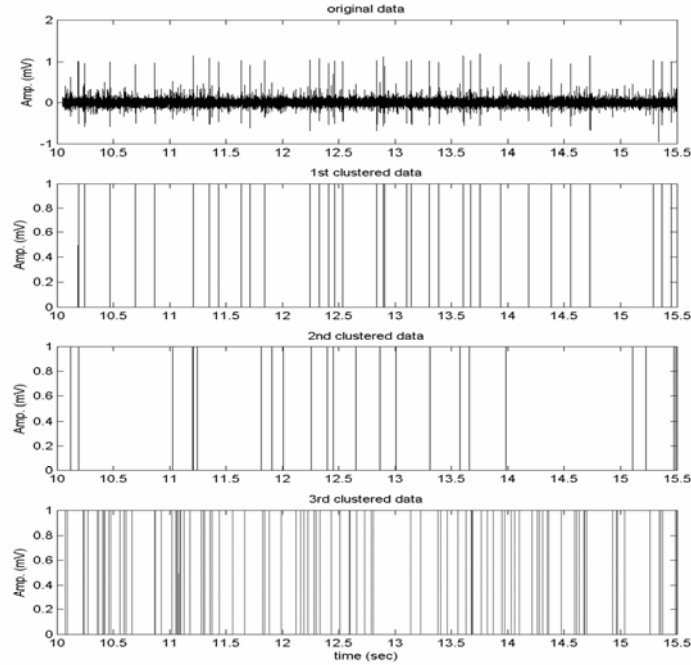


Figure 3.14. The original neuron signal (top) and the firing times for each neuron (the rest)

For the verification of the classification by variance estimation, Figure 3.15 shows histograms of heights with variance estimations by the Levenberg-Marquardt method. The smaller hump on the right side of the upper figure demonstrates falsely detected data caused by applying the simple Euclidean distance. .

3.4. Discussion

As we can see in the flow chart for the whole system shown in Figure 3.16, the directions of firings and number of spikes based on the spike shapes can be

confirmed by users. It is known that neuronal firings are recorded in one direction, positive or negative, on an electrode [28], which means that spikes with different directions must be considered to be different neurons. This method is for classifying neurons in the same direction. Furthermore, since the neural system is so sensitive that a lot of noise may produce unwanted dominant principal components, our system offers the semi-automated spike pickup interface. Figure 3.17 shows our user interface for the semi-automated spike pickup interface. The system was implemented in Matlab 7.1 on the Windows operating system.

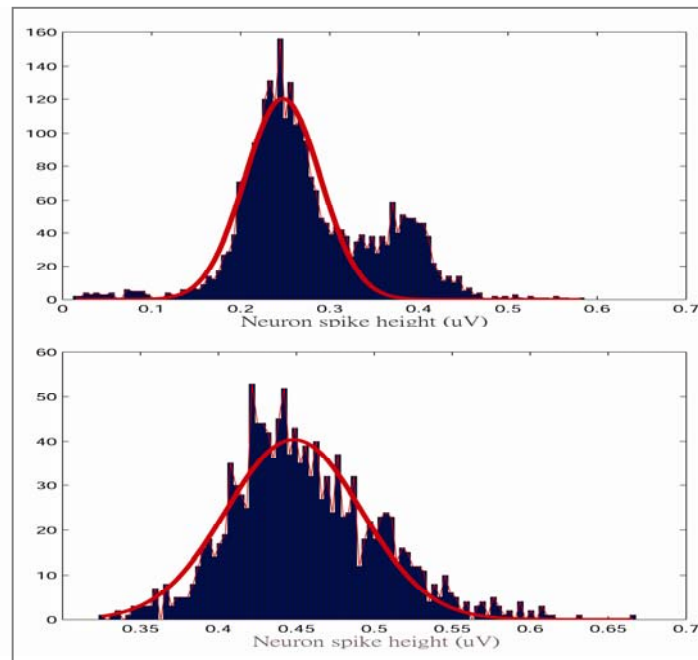


Figure 3.15. Variance estimation on real data by applying the Levenberg-Marquardt method (below) to data previously classified by a Euclidean metric (above).

Although neuron spike sorting has been used for brain activity research and several methods have been proposed and used, none of the prior techniques satisfy our requirements. The main problem is that neural signals have a great deal of noise and the shapes of spikes are extremely diverse. Our method uses the maximal overlap discrete wavelet transform for de-noising without shape distortion and rotated principal component analysis for extracting spike

templates, which overcomes the limitation of orthogonality of the PCA method and is a good solution for spike sorting. Furthermore, since the template matching by a Euclidean metric can cause classification errors due to widely differing variances, the proposed method uses the Levenberg-Marquardt algorithm to estimate the variances of each cluster based on distribution shape, and a weighted Euclidean metric to refine the classification results. The new method improves clustering, even when the heights of the neuron classes are too close to measure variances by existing statistical estimation methods.

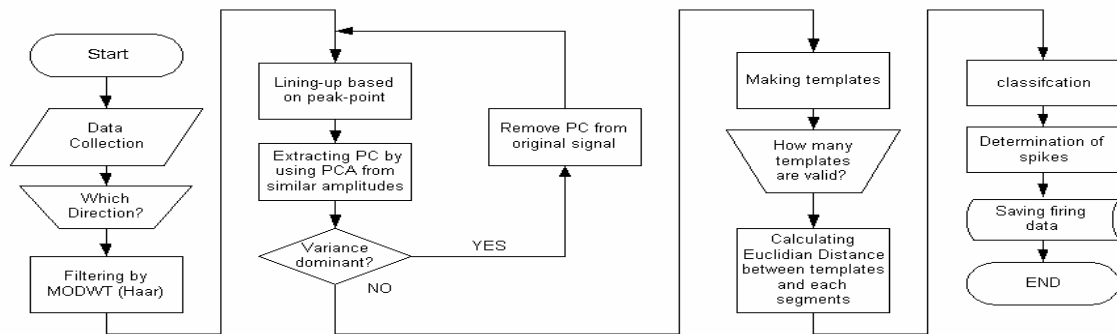


Figure 3.16. Flow chart

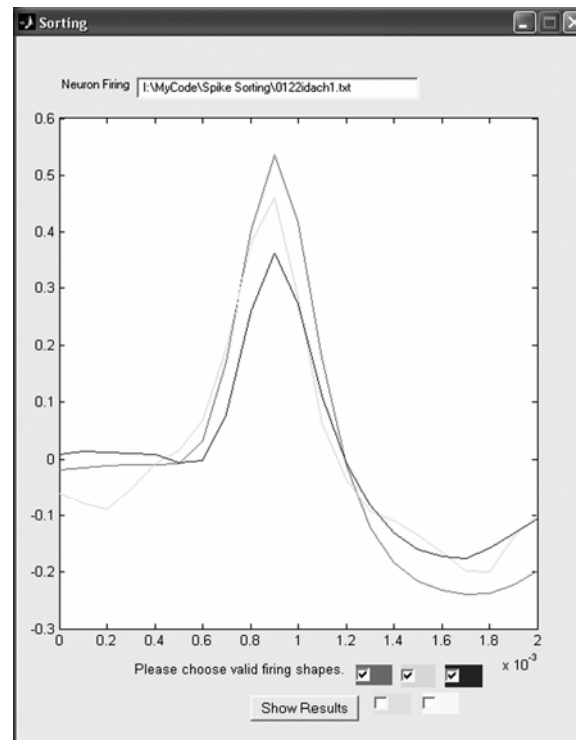


Figure 3.17 Semi-automated user interface for selecting valid neuron spikes by experts.

Chapter 4

CHARACTERIZING NEURONAL FIRING PATTERNS IN THE HUMAN BRAIN

4.1. Introduction

Neuroscientists and cognitive neuroscientists, who are studying the single neuron cell activities of the human brain, are currently interested in at least two different applications. The first application is to determine if there are any pattern similarities across the specific events. Until now, only the second order statistics of neuron firings have been considered to check those similarities. However the second order statistics cannot provide any information about shape changes in either the temporal domain or the frequency domain. So a new method to characterize neuron firing patterns is necessary. The second application is in content-based retrieval systems that can compare specific results to a database of human brain images and retrieve data similar to these in a query. Functional Magnetic Resonance Imaging (fMRI) images, as well as neuron firing signals, can be used as 'content' for the query system. However, since file sizes for both fMRI and neuron firings are too big to be uploaded on a server for full online comparisons, an efficient indexing method is also required. If we can characterize neuron firing templates that occur frequently and assign each firing pattern to the closest class, the firing pattern classes can be used for indexing and efficient access.

To define neuron firing pattern profiles, we are investigating two approaches. The first one is to classify the firing patterns in the frequency domain, in which an eighth order sine multitaper spectral estimator and a ninth degree polynomial curve fitting are used. The second one is to characterize the firing patterns in the time domain, in which local maxima of the signals are

measured, and a cubic spline interpolation is applied to get smooth variations in time.

To extract suitable templates from the human brain neuron signals themselves, the rotated principal component analysis (RPCA) is used, and to compare the neuron firing signals with the templates generated by the RPCA regardless of errors due to data shift or amplitude changes, the dynamic time warping method is employed to efficiently find the shape similarities.

4.2. Data

Electrophysiological recordings were obtained during neurosurgery performed by Dr. George A. Ojemann in the Neurosurgery Department, University of Washington. During neurosurgery for intractable epilepsy, patients were asked to respond to 63 audio, picture, or text stimuli with some stimuli being repeated. For each patient, four electrodes were placed in the temporal lobe to collect neuronal firings extracellularly. Each neuron was discriminated using an amplitude-frequency histogram, and the raw number of the neuron spikes per 50 millisecond bin was accumulated in a three-second period.

4.3. Methodology

4.3.1. Firing patterns in the power spectrum

To obtain frequency profiles, the raw temporal firing signals were adjusted to zero mean and zero-padding with 120 zeros to enhance the visualization. The zero-padded raw time signals were characterized using sine multitaper spectral estimation. This technique is used to estimate power spectra, and it works automatically on high dynamic range spectral density functions. Although parametric estimation methods also produce smooth shapes, they are not

suitable for these data, since the characteristics of the data are not known. As a nonparametric estimator, the multitaper spectral estimator is the average of K direct spectral estimators:

$$\hat{S}^{(mt)}(f) = \frac{\Delta t}{K} \sum_{k=0}^{K-1} \left| \sum_{t=1}^N h_{t,k} X_t e^{-j2\pi f t \Delta t} \right|^2 \quad (4.1)$$

where $\{h_{t,k}\}$ is the k th taper. The $K=8$ sine multitaper method, due to small variance and acceptable bandwidth, was used for this project, with the k th tapers defined as [27]

$$h_{t,k} = \left\{ \frac{2}{N+1} \right\}^{1/2} \sin \left\{ \frac{(k+1)\pi t}{N+1} \right\} \quad (4.2)$$

Figure 4.1 shows the examples of comparing the multitaper spectral estimation method with Hanning windowing and with the autoregressive (AR) model. As shown in the figure, the AR model does not coincide with the nonparametric methods, which makes the parametric method improper for estimating power spectra of neuron firings.

Even though the multitaper power spectral estimations can produce smooth curves in the spectral domain, there are still some ripples that make it hard to extract common firing patterns for indexing in a retrieval system. To obtain smoother patterns, the 9th degree polynomial curve fitting method is applied to the multitaper power spectral estimation results. The polynomial curve fitting generates the minimum least square errors of any curve-fitting method for these neuron firing signals. The 9th degree is large enough to deal with any firing patterns in the spectral domain. Polynomial models are given by $y = \sum_{i=0}^n p_i x^{n-i}$,

where n is the order of the polynomial, n is the degree of the polynomial, and $n=9$ here. The order gives the number of coefficients to be fit.

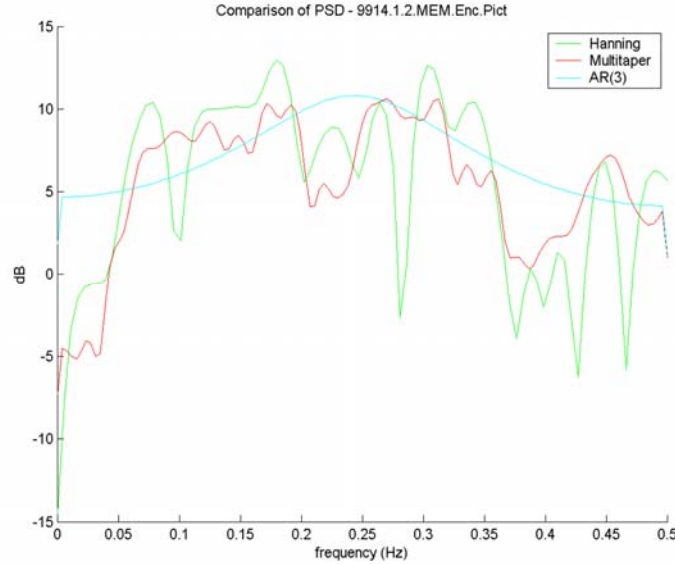


Figure 4.1. The comparison of multitaper spectral estimator (red) with Hanning windowing method (green) and Autoregressive models (cyan)

4.3.2. Firing patterns in the temporal domain.

The raw temporal data that is obtained by summing the number of spikes in every 50msec window were further profiled using eight point local maxima to acquire rough changes of signals in the temporal domain. Based on experimental results, eight points were sufficient to obtain temporal patterns. These eight points were smoothly connected by a cubic spline interpolation method:

$$y = Ay_j + By_{j+1} + Cy_j'' + Dy_{j+1}'' \quad (4.3)$$

where $y_i = y(x_i)$, $i = 1, \dots, N$, the y 's are the particular interpolations between y_j

and y_{j+1} , and the coefficients are $A = \frac{x_{j+1} - x}{x_{j+1} - x_j}$, $B = 1 - A = \frac{x - x_j}{x_{j+1} - x_j}$,

$C = \frac{1}{6}(A^3 - A)(x_{j+1} - x_j)^2$, and $D = \frac{1}{6}(B^3 - B)(x_{j+1} - x_j)^2$ [28]. The cubic spline interpolation of the local maxima produces smooth firing patterns in the temporal domain.

4.3.3. Classifying firing patterns.

About 4100 firing patterns were collected by applying the methods mentioned above in both the temporal domain and the spectral domain. Each firing pattern signal was normalized to allow efficient shape comparison. The normalization is given by

$$X'_j = X_j / \sqrt{\sum_{i=1}^M X_i} , \quad j = 1, \dots, M \quad (4.4)$$

where X_j is the j th element of the firing pattern signals, and X'_j is the j th normalized signal. Then the rotated principal component analysis (RPCA) method was employed to extract the most common firing patterns based on the experimental data themselves. As stated in Chapter 3, the RPCA can extract templates overcoming the orthogonality limitation of the traditional PCA. For these human brain neuron firing signals, the first eight primary principal components accounted for over 95% of the variance and were used for subsequent classifications. The same procedure was used to provide eight templates for both the spectral domain and the temporal domain. Figure 4.2 shows the eight templates for spectral domain, and Figure 4.3 shows the templates for temporal domains.

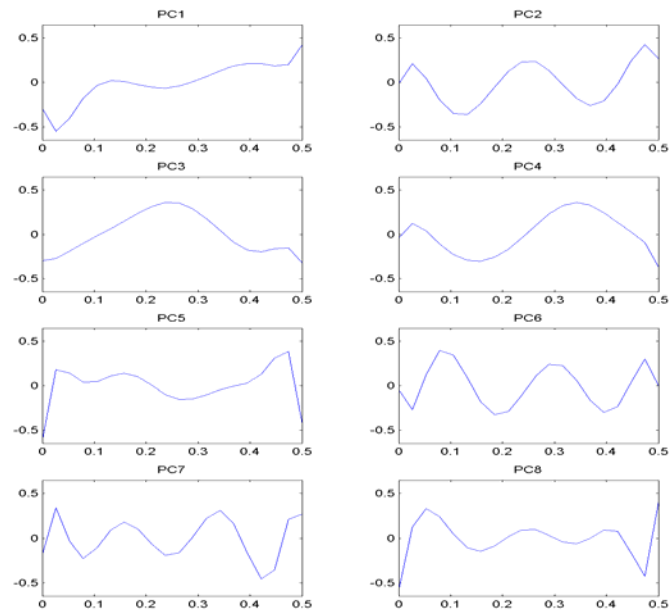


Figure 4.2 The eight templates for the neuron firing patterns in frequency domain. X-axis is the normalized frequency and y-axis is normalized amplitude

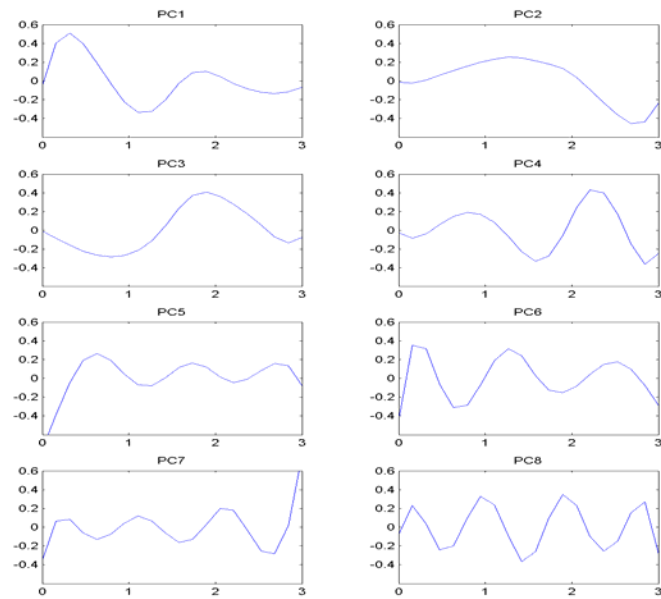


Figure 4.3 Eight templates for the neuron firing patterns in temporal domain. X-axis is time (second) and y-axis is normalized amplitude

Based on each of the eight templates extracted in both the temporal domain and the spectral domain, each signal from each event can be assigned to the closest class by comparing them with templates. However, simple comparison methods like cross correlation may cause huge errors when comparing even slightly shifted inputs. To compare patterns of firing similarity between neurons and to avoid the errors caused by shifted signals, we used the dynamic time warping (DTW) procedure to categorize a given neuronal response for a single trial to the closest fitting template. This procedure strives to produce a match between the raw single trial signal and one of the eight templates. The template that results in the lowest cost function is considered to be the best match. The cost function D can be expressed as

$$D(i, j) = \sum_{k=0}^{K-1} d(i_k, j_k) \quad (4.5)$$

where k is the number of nodes along the path in the grid [3]. Considering that the characteristics of neural signals do not change excessively, the end-point constraint as well as the one-step constraint was taken into account to get the best results as in Chapter 2.

Given these data driven categorizations we are in a position to objectively compare the similarity of neurons sampled from within a single electrode, or between two electrodes on a single microdrive, or between two microdrives.

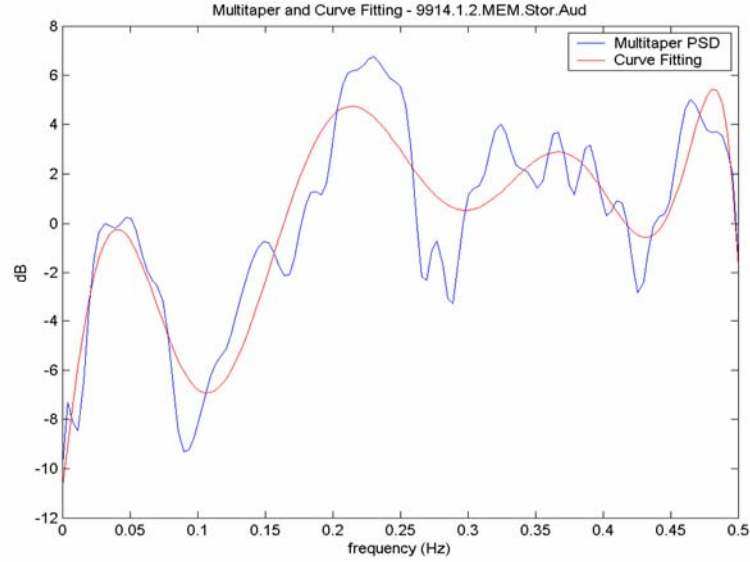


Figure 4.4 An example of multitaper spectral estimation (blue) and its ninth degree curve fitting result (red).

4.4. Results

The proposed method has been applied to the neuron signals recorded from the temporal lobes of human subjects. Around 4100 event firing signals from 42 neurons in 12 patients were processed to extract firing templates in both the temporal domain and the frequency domain.

To obtain the firing patterns in the power spectrum, the raw data with spikes accumulated every 50 msec, adjusted to zero mean and eighth order sine multitaper power spectral estimation, was applied, followed by ninth degree polynomial curve fitting. Figure 4.4 shows an example of multitaper spectral estimation and ninth degree polynomial curve fitting.

The neuron firing patterns in the temporal domain were acquired by smoothly connecting eight local maxima with cubic spline interpolations. Figure 4.5 shows examples of firing patterns in the temporal domain. As shown in

Figure 4.4 and Figure 4.5, the information about approximate changes in time is represented in the temporal domain, while the information about fluctuation is denoted in the power spectrum.

The neuron firing templates were extracted by the rotated principal component analysis, as discussed in Chapter 3. Each of the eight templates in time and in the power spectrum was compared with each neuron firings to classify them using the dynamic time warping method. Figure 4.6 shows the use of the DTW to find the closest firing patterns. Initial classification of the database upon this method demonstrates that for a given subject, pairs of neurons sampled from a single electrode showed more similarity in firing patterns than those sampled from different electrodes, this finding is consistent with known models of cortical organization.

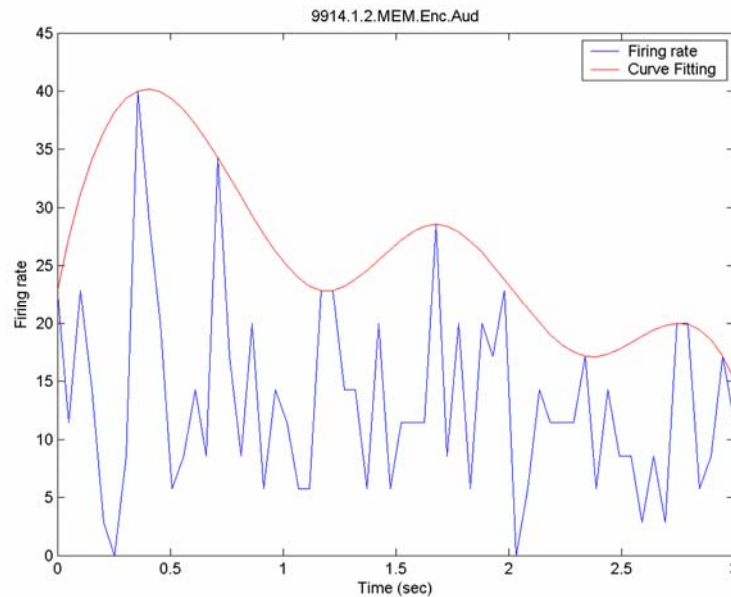


Figure 4.5 An example of finding local maxima and cubic spline interpolation result (red).

4.5. Discussion

Although the dynamic time warping method can find the closest class for each neuron firing, it is very hard to assign intermediate shapes to only one specific class, and this may cause errors in the query system. To avoid that kind of error, the neuron firing patterns will have the closest class as the first index, the second closest class as the next index, and the third one as the next. The distances by the DTW for these three pattern numbers are also saved as weights to maximize the efficiency of the querying procedures. In the query system, a refined algorithm will be used based on the indices and weights.

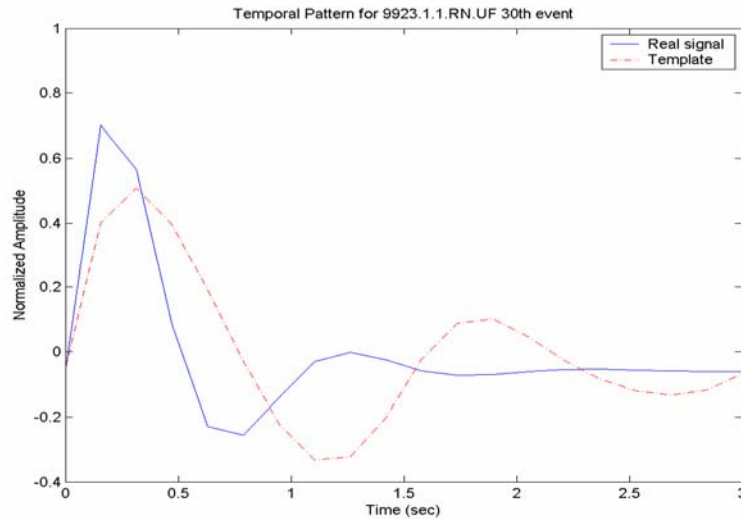


Figure 4.6 An example of finding the closest class by DTW

Although there are numerous needs for characterizing the firing patterns for human brain neuron signals, only the second order statistics have been used to find firing similarities. To make matching and retrieval of functional brain data efficient, the neuron firing patterns should be categorized into appropriate templates extracted from human brain neuron signals.

Several methods to characterize the variations in both the temporal domain and frequency domain of neuron firing shapes were proposed. The rotated PCA was used to extract firing templates overcoming the orthogonality limitation. To assign each neuron firing to the closest class while minimizing the shift error, the dynamic time warping method was used, and the second and the third closest classes were also saved as weight vectors. The indices and weight vectors along with means and variances of the neuron firings will be utilized to find pattern similarities and to develop an effective query algorithm.

Chapter 5

QUERY SYSTEM FOR CONTENT-BASED RETRIEVAL OF HUMAN BRAIN DATA

5.1. Introduction

The goal of a content-based retrieval system is to efficiently query and retrieve data from a database that have similar characteristics to those of the query. In order to this, appropriate features have to be extracted from the data and used as indices for retrieval. In our system, features of single unit recordings and fMRI in both the temporal and the spatial domains are characterized and indexed.

Our data comes from studies of epilepsy patients who undergo neurological surgery at the University of Washington. Each subject has three types of information: patient information, single unit recording results, and fMRI activation information. The patient information consists of the patient's name, sex, age, disease, patient number, and surgery date. The single unit recording information has an electrode number and a neuron number; the neuron has corresponding firing patterns along with weights for specific tasks. The functional MRI activation data is associated with the same tasks and events as the memory task which is performed in the single unit recording. These three types of information lead to the indices in our systems.

5.2. Common features for both single unit recording and fMRI data

In a content-based retrieval system especially for human subjects, common features of both fMRI and single unit recordings would be used as indices. The basic common factors are patient information such as name, sex, surgery date,

patient number, and fMRI experiment number. Table 5.1 shows the index of basic patient information.

Table 5.1 Index of basic patient information

Index	Description
PNum	Patient Number
ENum	fMRI Experimental Number
Name	Patient Name
Date	Surgery Date
Sex	Patient Sex
Age	Patient Age

Furthermore, cognitive trial protocols, which are administered to patients to quantitatively measure brain activities, are also used as indices. Specific cognitive experimental protocols are used on a patient to associate brain activities in the fMRI with the single unit recordings. There are five kinds of experimental design protocols for a single unit recording:

- (1) **Memory load:** a trial protocol to look at the effect of load on memory. Neuronal activity in an identification task is compared to activity from the memory task. Subjects are asked to name and remember 1, 3, or 5 items. After a set of distracter items, subjects are asked to recall the original items.
- (2) **Temporal delay:** a trial protocol similar to the memory load for 1 or 5 items. However, a temporal component is added to test the effect of temporal delay on memory. Short (10 seconds) or long 60 second delays are added during the distracter items, before the subject is asked to recall.
- (3) **Paired associates:** a trial protocol to compare neuronal and fMRI activity with a paired associate test. Following a 21 second fixation period,

subjects are asked to either identify a word or identify and remember word pairs. There are 8 trials in each block (1 ID, 2 PA blocks).

- (4) **Implicit/explicit:** a trial protocol to compare the difference in neuronal activity between identification and memory tasks. Subjects are given a Brown-Peterson memory task in which they are asked to identify and remember a word, followed by either a distracted or non-distracted period, after which they are asked to recall the word. This is compared to an identification task in which the subject is asked to identify the item.
- (5) **Blocked design:** a trial protocol similar to temporal delay, except that identification and memory blocks are grouped according to either short or long delay items.

Only two of the five protocols — paired associates and memory load — are used as protocols for fMRI experiments. Table 5.2 shows the index of protocols for single unit recording and fMRI data.

Table 5.2 Index of protocols for single unit recording and fMRI data

Index	Protocol for SUR	Protocol for fMRI
P_ML	Memory Load	Paired Associates
P_TM	Temporal Delay	Memory Load
P_PA	Paired Associates	_____
P_IE	Implicit/Explicit	_____
P_BL	Blocked	_____

For each experimental protocol, there are several kinds of trial tasks — identification, encoding, storage, retrieval, fixation, and so on. Additionally the trial tasks are sometimes modified by cognitive scientists for specific research purposes. For instance, in the identification task, patients are asked to identify what they recognize, while in the storage task, they are requested to remember

what they see. In the retrieval protocol, subjects are asked to say what they remember from something they have previously seen or heard. Table 5.3 shows the Index of trial tasks for single unit recording and fMRI data.

Table 5.3 Index of trial tasks for single unit recording and fMRI data

Index	Trial tasks for SUR	Trial tasks for fMRI
T_Pix	Fixations	Fixations
T_Enc	Encoding	Encoding
T_Stor	Storage	Storage
T_Ret	Retrieval	Retrieval
T_Intv	Interval	Interval
T_Id	Identification	_____

In each study, a subject is asked to respond to stimuli which are given in the forms of audio, picture, and text. These stimulus modalities are also used as common features for indices for both single unit recording and fMRI data.

5.2.2. Single unit recording features

Action potentials from one neuron contain firing information according to each stimulus applied. The information from neuron firings is characterized by features for the content-based retrieval system in both the spatial and the temporal domains.

5.2.2.1. Spatial features of SUR

Locations of microelectrodes are the most important aspect of spatial characteristics of single unit recordings. They are represented in two ways: 1) a Euclidean coordinates in a canonical brain system; 2) section in a brain parcellation scheme. For cross-patient research, each brain image has to be

registered to a canonical brain system such as Montréal Neurological Institute (MNI) coordinates or Talairach coordinates. The x , y , and z coordinates on the canonical image are saved as spatial indices.

The second way to represent the microelectrode location is the brain parcellation scheme which has been developed by the Structural Informatics Group, University of Washington for the study of cortical stimulation mapping. The parcellation has been called an “anatomical labeling for cerebral cortical stimulation (CSM) sites which is necessary for intelligent computer querying for a rich and unique experimental database examining neural substrates underlying human language production.” [29]. Figure 5.1 shows the brain anatomical parcellation scheme.

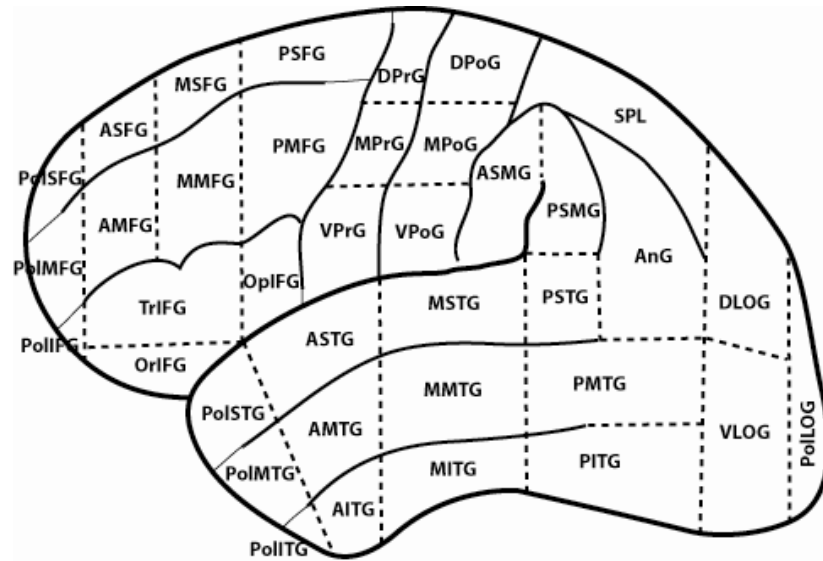


Figure 5.1 the brain anatomical parcellation scheme

The parcellation labels can be used as features of the microelectrode locations for retrieval. To map the microelectrode sites to the canonical brain volume or to the anatomical parcellation scheme, MNI_AutoReg software [30] is used with expert verification [31]. Table 5.4 shows the index of spatial features for single unit recording data.

Table 5.4 Index of spatial features for single unit recording data

Index	Description
RLM	Rough Location of Microelectrode in Parcellation scheme
SLM	Specific Location of Microelectrode (ex. 3 mm from MMTG ¹)
DM	Depth of Microelectrode
MX	X coordinate of Microelectrode
MY	Y coordinate of Microelectrode
MZ	Z coordinate of Microelectrode

5.2.2.2. Temporal features of SUR

Temporal aspects of neuron spike information are expressed in the form of firing rate, firing time pattern and firing frequency pattern, and the corresponding probabilities. The firing rate is the average number of neuron spikes in a specific time period. Firing patterns are extracted using several signal processing techniques. As discussed in chapter 4, several methods to characterize the firing patterns of the neuron spikes from human brain both in temporal domain and frequency domain have been developed.

The combination of multitaper spectral estimation and a polynomial curve fitting method is employed to produce the firing patterns in the frequency domain. To generate temporal shapes, eight local maxima are smoothly connected by cubic spline interpolation. A rotated principal component analysis, which removes the orthogonality constraints of traditional PCA is used, to extract common firing patterns as templates from around 4100 neuron spikes. Dynamic time warping is used to assign each neuron firing to the closest template without shift error [2]. Furthermore, to minimize the error caused by

¹ One of names of parcellation scheme in Figure 5.2

assigning neuron characteristics to just one specific class, the first and the second closest classes are also saved as feature vectors. The indices and their probability vectors, along with the statistical means of the neuron firings, are utilized to find pattern similarities and to develop an effective query algorithm. Table 5.5 shows the index of temporal features for single unit recording data.

Table 5.5 Index of temporal features for single unit recording

Index	Description
FR	Firing Rate
TP	Time Pattern
FP	Frequency Pattern
TPPr	Probability of Time Pattern
FPPr	Probability of Frequency Pattern

5.2.3. fMRI features

Since the size of the file containing fMRI activation results is very large for the content-based retrieval system, some features of the activations have to be extracted and saved as indices for efficient queries. The characteristics of fMRI activations are also represented in both temporal and spatial terms.

5.2.3.1 Spatial features of fMRI

With regard to the spatial features, the most highly activated positions in a 3-D volume have x, y, and z coordinates in a canonical brain image, similar to the single unit recording case. Furthermore, since the fMRI activations are compared to the characteristics of single cell recording, the 3-D activation points have to be mapped onto the brain surface. For this task, we use the Brain Visualizer [32] developed by the University of Washington Structural Informatics Group. For 3-

D volume to brain surface mapping, two methods are used in the Brain Visualizer. The first method highlights the surface areas that are located in close vicinity to the fMRI activations. The alternative method is that activation anywhere in the brain is projected onto the surface, using the projection points from the center point in the magnetic coordinate² to anterior commissures³ [31]. In addition, to make the query system more precise, the second or third mostly activated locations are also saved as spatial indices. Other features of fMRI in the spatial domain include activation sizes as numerical ranges as well as the number of activations in the most activated location. Table 5.6 shows the index of spatial features for fMRI data.

Table 5.6 Index of spatial features for fMRI data

Index	Description
LA1	Location of the most Activation in Parcellation scheme
LA2	Location of the second most Activation in Parcellation scheme
SA	Size of Activation in the most activated location
NA	Number of Activation in the most activated location
MfM	Mean value of fMRI activation
fX	X coordinate of fMRI (highly activation)
fY	Y coordinate of fMRI (highly activation)
fZ	Z coordinate of fMRI (highly activation)

5.2.3.2 Temporal features of fMRI

For temporal features of fMRI, normalized intensities and delay times of hemodynamic responses at the corresponding activation locations are applied. The delay time of the hemodynamic response is about 2 seconds. Therefore, if the

² A coordinate system centered at the middle point in fMRI scanner

delay time is between 1.5 and 2.5 seconds, it is assigned to 'normal'. If the delay time is less than 1.5 seconds, it is considered a 'fast' response, while if it is more than 2.5 seconds, it is assigned the status 'slow'. In addition, hemodynamic response vectors at the most activated sites are saved as temporal features of fMRI. The hemodynamic response vector consists of approximately 20 floating numbers. Table 5.7 shows the index of temporal features for fMRI.

Table 5.7. Index of temporal features for fMRI data

Index	Description
HRA	Amplitude of Hemodynamic Response
HRD	Delay of Hemodynamic Response
HR	Hemodynamic Responses

Figure 5.2 shows the data structure of the indices for the content-based retrieval system.

³ A tract of nerve fibers passing from one side to the other of the spinal cord or brain

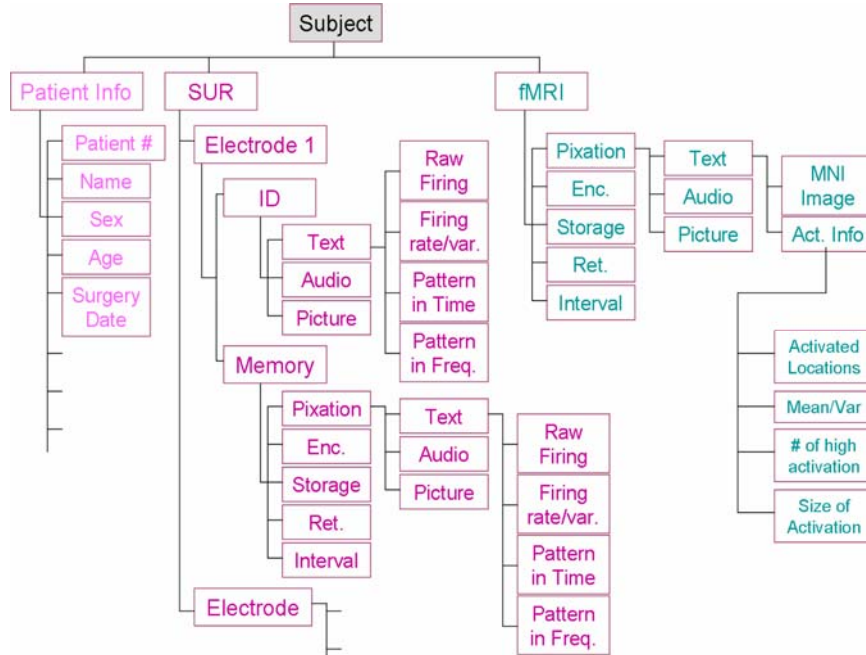


Figure 5.2 Data structure for the content-based retrieval system.

5.3. Query algorithm and graphical user interfaces

Since the data used in the content-based retrieval system for functional human brain researches contains complicated spatio-temporal relationships in both SUR and fMRI data, an efficient query algorithm has to be developed. Since we expect that a brain location having a significant activation in the fMRI also has a noteworthy neuronal firing pattern in the single unit recording for a specific trial protocol, shared features of fMRI and SUR in both the temporal and spatial domains (brain location, trial protocol, patient information) play important roles in query algorithms.

To verify the functionality of a content-based retrieval system for functional human brain signals, a graphical user interface is implemented. These datasets were constructed for testing purpose.

1) a single unit recording dataset, which contains the basic patient information (patient number, patient name, sex, age, surgery date), spatial information (location and depth of microelectrode), temporal information (firing time patterns, firing frequency patterns, firing rate), and trial protocol information,

2) an fMRI dataset, which consists of temporal features (amplitude and delay ranges of hemodynamic responses, hemodynamic response vectors) and spatial features (locations and sizes of hemodynamic responses) and the corresponding patient information and trial protocols, and

3) a Cortical Simulation Mapping (CSM) dataset, which contains the locations on the brain surface of points associated with both fMRI and SUR.

These three datasets are stored separately, but the user interface program controls them, combines them and uses them as indices. The basic patient information is used as a common feature to link the single unit recording dataset with the fMRI dataset. Figure 5.3 shows the file structures for the graphical user interface.

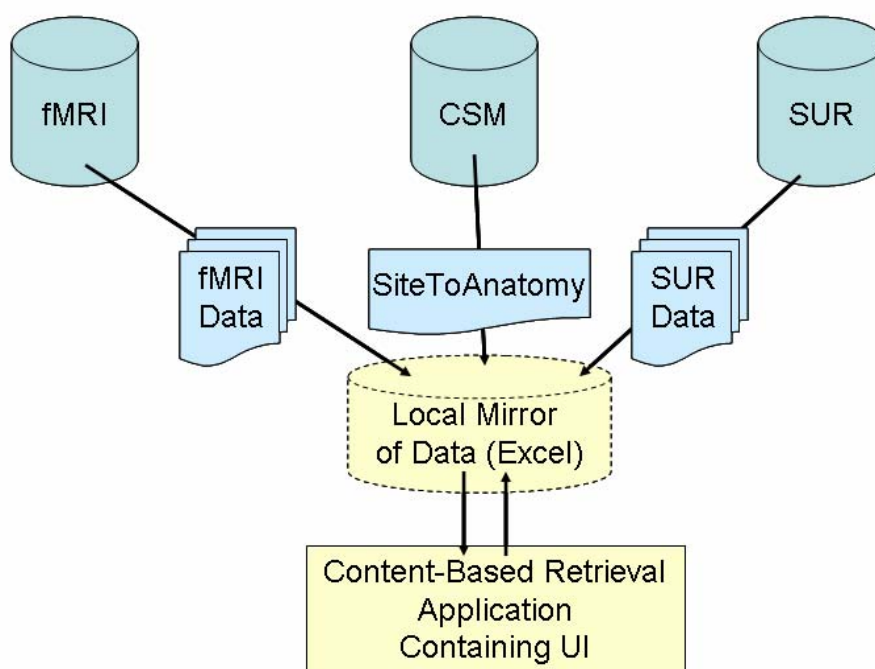


Figure 5.3 A file structure for the graphical user interface implementation

5.3.1. Search routes

The human brain information will be stored in a database for which a variety of queries will be implemented. Queries can include patient information, trial protocols applied to the patients, fMRI activation indices, neuron firing pattern indices with probabilities, or combinations that have been discussed earlier. Figure 5.4 shows the relationships of each search route: 'patients' have experiments with appropriate 'trial protocols', by which fMRI and SUR data are collected. The fMRI activations are then detected and the results are saved for retrieval, while single unit recording data are spike-discriminated first and their features are also stored in the database.

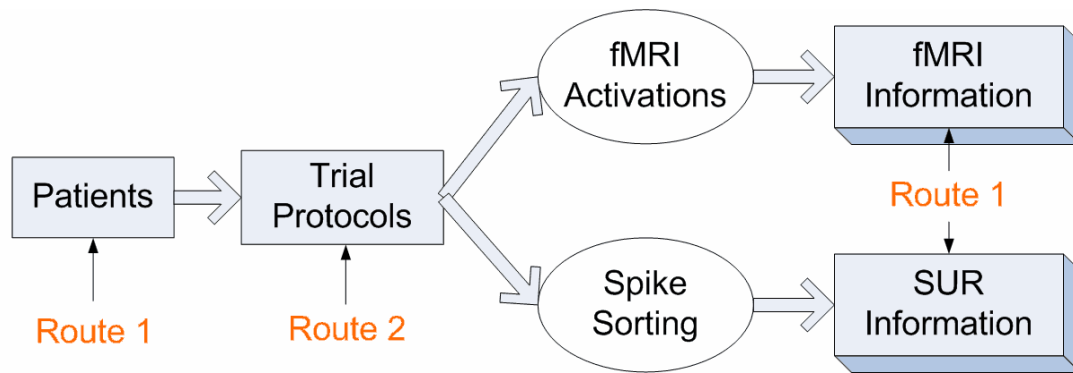


Figure 5.4 A diagram of search routes for the content-based retrieval system for functional human brain.

In the graphical user interfaces, users of the CBIR system view an initial screen from which they can select one of three search routes — 1) query by patient information, 2) query by trial protocol, 3) query by firing patterns and/or fMRI activations. Figure 5.5 is a screen shot of the initial screen.

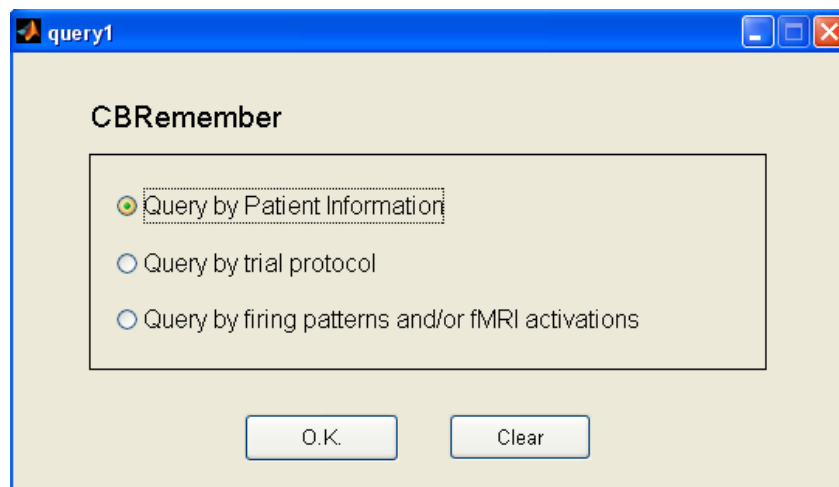


Figure 5.5 A screen shot of the initial search route selection

In the next several sections, the form of each major type of query will be defined. The syntax will be given in Backus-Naur Form (BNF) notation. The semantics will be described in English. All queries have the form:

$$\begin{aligned}
 <query> \rightarrow <information\ specification> <command> \\
 <information\ specification> \rightarrow <specification\ 1> | <specification\ 2>
 \end{aligned}$$

|.....|<specification N>

5.3.2. Query by basic patient information

The first type of query is based on patient information keys such as patient surgery number, age, sex, surgery date, or fMRI number. The patient queries can return information in the form of text only, SUR raw data, or fMRI images. For example, if a user wants to query the database by patient age alone, the retrieval system will make a list of corresponding surgery dates, surgery numbers, single unit recording raw firing data, or fMRI activation data, so the user can select patients to query more deeply. Figure 5.6 shows a rough idea of the query by basic patient information.

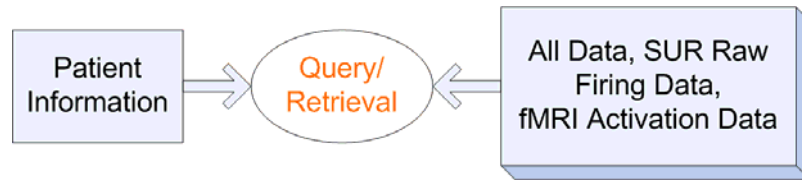


Figure 5.6 Query route by patient information

The patient information query route can be expressed in BNF as follows.

```

<patient_info_spec> → <basic_patient_spec> | <basic_patient_spec>
                        <patient_info_spec>
<basic_patient_spec> → <patient_no> | <age_range> | <sex> | <surgery_date> |
                        <fmri_no>
<patient_no> → <neuronal_surgery_number>
<age_range> → <age_number-age_number>
<sex> → <male | female>
<fmri_no> → <biostructures_fmri_number>
  
```

The patient queries can return information in the form of text only, SUR raw data, or fMRI images.

$\langle \text{patient_info_query} \rangle \rightarrow \langle \text{patient_info_spec} \rangle \langle \text{command} \rangle$
 $\langle \text{command} \rangle \rightarrow \text{"all"} \mid \text{"text_only"} \mid \text{"SUR raw dat"} \mid \text{"fMRI image"}$

5.3.2.1. Query by patient information with SUR characteristics.

If the query by patient information is combined with single unit recording characteristics such as number or location of microelectrodes, then the corresponding firing rates, firing patterns or trial information is retrieved, instead of raw data. Figure 5.7 shows an example query route by basic patient information with the microelectrode/neuron number specified.



Figure 5.7 Query route by basic patient information with microelectrode / neuron number

After selecting a patient number, users can also choose one of the microelectrodes and neurons, by which neuron firing information with trial protocols are retrieved as a table. Query by patient information with microelectrode/neuron number is expressed in Backus Naur Form below.

$\langle \text{patient_info_with_sur_neuron_no_query} \rangle \rightarrow \langle \text{trial_protocol} \rangle \text{"activate"}$
 $\langle \text{neuron_firing_electrode} \rangle$
 $\langle \text{trial_protocol} \rangle \rightarrow [\langle \text{pixation} \rangle \mid \langle \text{encoding} \rangle \mid \langle \text{storage} \rangle \mid \langle \text{retrieval} \rangle \mid \langle \text{interval} \rangle]$
 $[\langle \text{text_stim} \rangle \mid \langle \text{audio_stim} \rangle \mid \langle \text{picture_stim} \rangle]$
 $\langle \text{neuron_firing_electrode} \rangle \rightarrow \langle \text{firing_info} \rangle \langle \text{firing_location} \rangle$
 $\langle \text{firing_info} \rangle \rightarrow [\langle \text{firing_rate} \rangle \langle \text{firing_var} \rangle] \mid [\langle \text{temporal_pattern} \rangle \langle \text{freq_pattern} \rangle]$
 $\langle \text{firing_rate} \rangle \rightarrow \langle \text{mean_of_firing} \rangle$
 $\langle \text{firing_var} \rangle \rightarrow \langle \text{variance_of_firing} \rangle$
 $\langle \text{temporal_pattern} \rangle \rightarrow \langle \text{primary_time_template} \rangle \langle \text{primary_prob} \rangle$
 $\langle \text{secondary_time_template} \rangle \langle \text{secondary_prob} \rangle$

$\langle freq_pattern \rangle \rightarrow \langle primary_freq_template \rangle \langle primary_prob \rangle \langle secondary_freq_template \rangle \langle secondary_prob \rangle$
 $\langle firing_location \rangle \rightarrow \langle mni_coord \rangle | \langle brodman_area \rangle | \langle parcellation_scheme \rangle$
 $\langle electrode_location \rangle \rightarrow \langle electrode_number \rangle \langle neuron_number \rangle$
 $\langle parcellation_scheme \rangle \rightarrow \langle PolSFG \rangle \langle ASFG \rangle \langle MSFG \rangle \langle PSFG \rangle \langle PolMFG \rangle$
 $\langle PollPG \rangle \langle AMFG \rangle \langle MMFG \rangle \langle PMFG \rangle \langle TriFG \rangle \langle OriFG \rangle \langle OplFG \rangle \langle DPrG \rangle$
 $\langle MPrG \rangle \langle VPrG \rangle \langle DPoG \rangle \langle MPoG \rangle \langle VPoG \rangle \langle ASMG \rangle \langle PSMG \rangle \langle SPL \rangle \langle AnG \rangle$
 $\langle DLOG \rangle \langle PolLOG \rangle \langle VLOG \rangle \langle PSTG \rangle \langle PMTG \rangle \langle PITG \rangle \langle MSTG \rangle \langle MMTG \rangle$
 $\langle MITG \rangle \langle ASTG \rangle \langle AMTG \rangle \langle AITG \rangle \langle PolSTG \rangle \langle PolMTG \rangle \langle PolITG \rangle$
 $\langle mni_coord \rangle \rightarrow \langle x, y, z \rangle$
 $\langle brodman_area \rangle \rightarrow \langle area_1 \rangle | \langle area_2 \rangle | \dots | \langle area_46 \rangle$

Time and frequency patterns consist of the 8 templates defined in Chapter 4; each neuron firing is assigned to the closest template. In addition, if users query the single unit recording information by common patient information spatially combined with the location of a microelectrode, then the resultant microelectrode/neuron number would be retrieved with the corresponding firing rates, time patterns, frequency patterns, and/or trial protocols. Figure 5.8 is a diagram of query and retrieval by patient information combined with the location of the microelectrode.

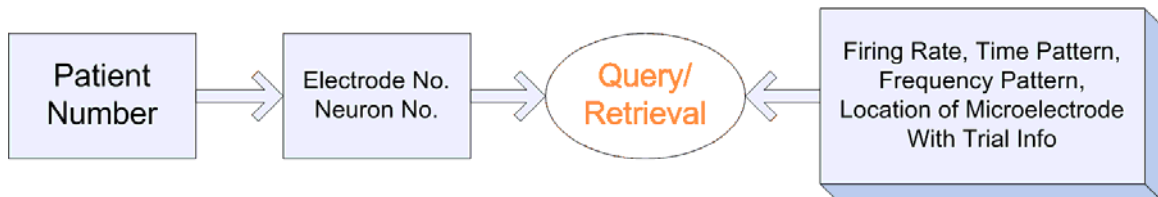


Figure 5.8 Query route by patient information combined with the location of the microelectrode

The query by patient information combined with the location of the microelectrode can also be expressed in Backus Naur Form notation below.

$\langle patient_info_with_sur_location_query \rangle \rightarrow \langle trial_protocol \rangle \text{ "activate"}$

$\langle neuron_firing_location \rangle$
 $\langle neuron_firing_electrode \rangle \rightarrow \langle firing_info \rangle \langle firing_location \rangle \langle electrode_info \rangle$
 $\langle electrode_info \rangle \rightarrow \langle electrode_number \rangle \langle neuron_number \rangle$

Examples of these kinds of queries will be demonstrated in the following graphical user interfaces.

When users want to query by basic patient information combined with fMRI characteristics, there can be two different ways to search: 1) temporal query and 2) spatial query.

5.3.2.2. Query by patient information with fMRI characteristics

The syntax of queries by patient information with fMRI characteristics is as follows:

$\langle fmri_activation_query \rangle \rightarrow \langle trial_protocol \rangle \text{ “activate” } \langle brain_area \rangle$
 $\langle brain_area \rangle \rightarrow [\langle mni_coord \rangle \mid \langle brodman_area \rangle \mid \langle parcellation_scheme \rangle]$
 $[\langle fmri_mean_var \rangle \mid \langle activation_size \rangle \mid \langle number_of_highly_activation \rangle]$
 $\langle fmri_mean_var \rangle \rightarrow \langle mean \rangle \mid \langle variance \rangle$
 $\langle activation_size \rangle \rightarrow \langle activated_area_size \rangle$
 $\langle number_of_highly_activation \rangle \rightarrow \langle number_of_activated_center_points \rangle$

5.3.2.2.1. Temporal query of fMRI activations with patient information

The fMRI data is retrieved by basic patient information with temporal features. Users can select the basic patient information, such as patient number or fMRI experimental number, and they are then able to choose trial protocols, amplitude range of hemodynamic response, and/or degree of hemodynamic response delay time. With this query request, the spatial fMRI features such as the location of the highest activation, and its size can be returned. Moreover,

users can query single unit recording characteristics related to this fMRI retrieved data. Figure 5.9 is a diagram of a query route for fMRI temporal query with basic patient information.

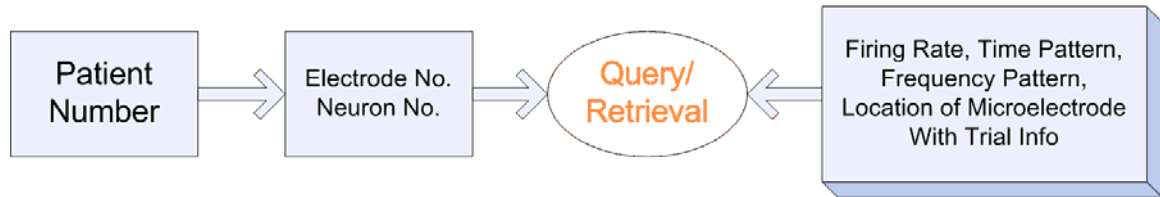


Figure 5.9 Query route by patient information combined with fMRI temporal features

5.3.2.2.2. Spatial query of fMRI with patient information

The fMRI data can be queried by spatial features such as the location of the highest activation and its size, by which corresponding trial protocols, amplitudes of hemodynamic response, and raw hemodynamic response vectors are retrieved. Users select one of the basic patient information indices, and choose the location of activation by clicking a position on the parcellation scheme or Brodman area map, selecting also the range of activation size. Figure 5.10 shows the query by patient information combined with fMRI spatial features

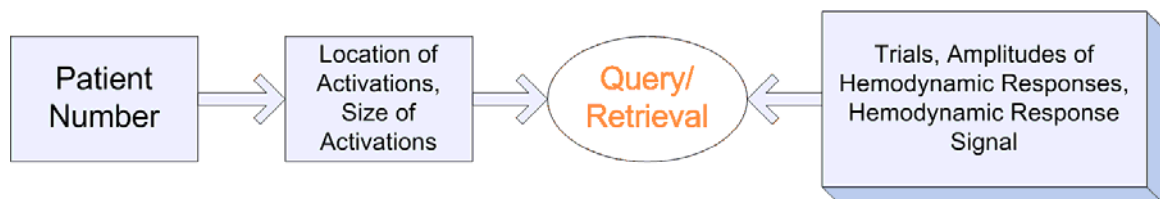
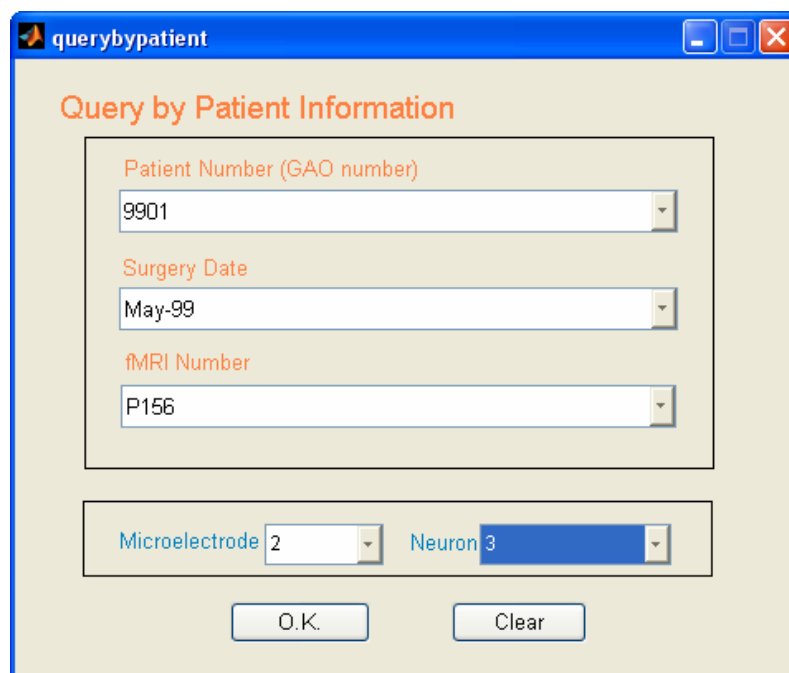


Figure 5.10 Query by patient information combined with fMRI spatial features

5.2.2.3. Graphical user interface for query by patient information

In the graphical user interfaces, if 'Query by Patient Information' is selected as a search route, users can choose a patient by one of the common features, that is, a patient number, a surgery date, or an fMRI number. To refine the retrieval

results, the microelectrode and neuron number can be specified. Different microelectrode and neuron numbers appear based on the different patient information. Figure 5.11 shows the selection of patient information and microelectrode/neuron number.



The screenshot shows a window titled 'querybypatient' with a blue title bar. The main area has a light beige background and is titled 'Query by Patient Information' in orange text. It contains two main sections. The first section, enclosed in a black border, contains three dropdown menus: 'Patient Number (GAO number)' with the value '9901', 'Surgery Date' with the value 'May-99', and 'fMRI Number' with the value 'P156'. The second section, also enclosed in a black border, contains two dropdown menus: 'Microelectrode' with the value '2' and 'Neuron' with the value '3'. At the bottom of the window are two buttons: 'O.K.' and 'Clear'.

Figure 5.11 Selection of patient information and microelectrode/neuron number selection

By selecting the patient number and microelectrode/neuron number, related information (such as patient name, sex, age, the location of microelectrode in a canonical brain, and trial protocols applied to the patient) is retrieved and displayed. Furthermore, users can choose one of the trial protocols to query more information or see a list containing whole matching firing patterns with their probabilities as shown in the right bottom of Figure 5.12.

The 'choosingtrial' window is divided into four sections:

- Patient Information:** GAO Number 9901, Surgery date May-99, fMRI P156, Patient Name ccc, Sex F, Age 32.
- Electrode location:** MNI Coordinate X -67.5095 Y -10.1705 Z -23.2839, Tal. Coordinate X -60.8767 Y 15.1856 Z 13.068, Brodman Area 44 Range 7. A 'Show Brodman' button is present.
- Electrode Info:** Electrode 2, Neuron 3.
- Query by trials:** A dropdown menu showing 'book(A)' and a 'Firing Info.' button.

Figure 5.12 A screen shot for choosing a trial for further querying

If whole trials are selected to be displayed, a trial protocol list with firing time patterns, firing frequency patterns with their probabilities, and patient numbers is shown, as in Figure 5.13.

The 'Untitled' window displays a table of neuronal firings with the following data:

Event	Time Pattern	Prob 1	Freq. Pattern	Prob 2	p-number
apple(A)	2	55 %	3	59 %	9934
dog(T)	2	69 %	3	72 %	9901
balloon(P)	2	74 %	3	58 %	9912
car control(A)	2	65 %	3	57 %	9912
glass(T)	2	58 %	3	57 %	9913
balloon(P)	2	56 %	3	72 %	9914
apple control(A)	2	68 %	3	60 %	9915
nose(T)	2	61 %	3	54 %	9923
apple control(P)	2	58 %	3	56 %	9927
book(A)	2	58 %	3	54 %	9931
apple(A)	2	78 %	3	58 %	9931
dog(T)	2	74 %	3	55 %	9935
balloon(P)	2	68 %	3	56 %	9935

A 'Firing Info' button is located at the bottom of the window.

Figure 5.13 A screen shot displaying a list of neuronal firings with similar firing patterns.

If users select a specific trial they want to query, matching indices such as the average firing rate and firing patterns in both the time and frequency domains with their probabilities are retrieved. For visualization, firing patterns are displayed as graphs. Moreover, users can request similar results to the ones already retrieved and displayed by clicking one of two menus — 1) querying similar firing patterns in a single unit recording, or 2) querying related fMRI results if they exist. As shown in Figure 5.14, users can see all of the results retrieved in a page at once.

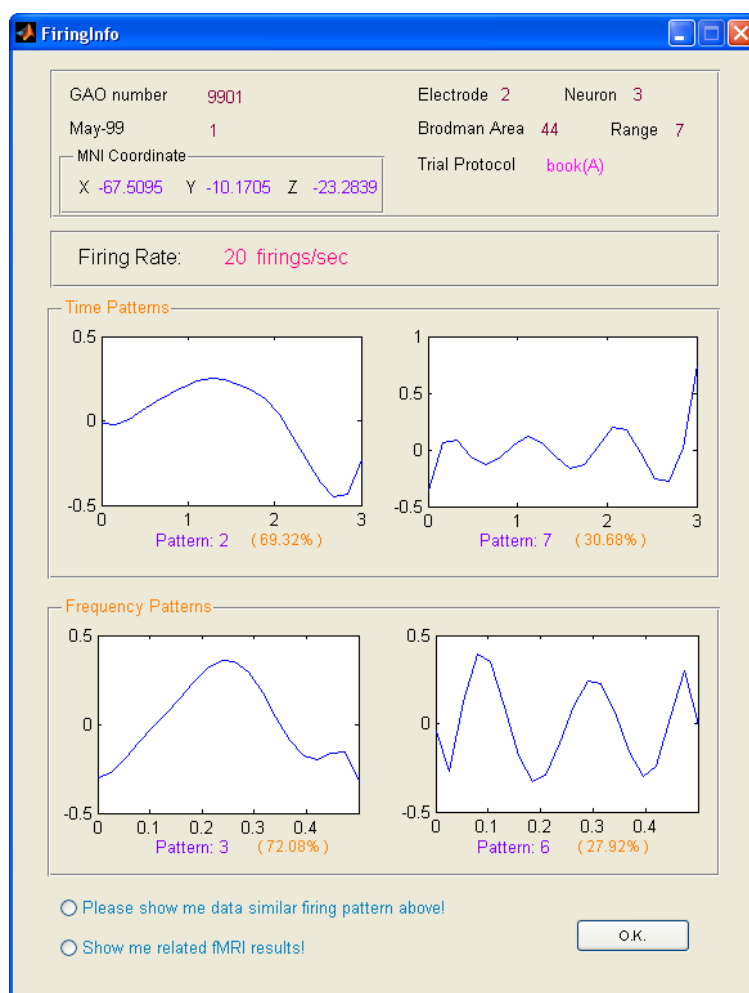


Figure 5.14 A screen shot displaying time and frequency patterns with their probabilities. A menu allows the user to extend the query by similar firing pattern or related fMRI results.

5.3.3. Query by trial protocols

The other search route is by trial protocols that have been defined earlier. While the query by patient information discussed in the previous section is done within a subject, users also want to find inter-subject characteristics from the database. For that query, similar characteristics of fMRI and SUR can be retrieved based on trial protocols. However, if trial protocols alone are used to query, the retrieved data is too huge to display appropriate results. Therefore, the searching routes are divided into three categories: 1) SUR, 2) fMRI, and 3) combination of SUR and fMRI.

5.3.3.1. Query by trial protocols of SUR characteristics

Since the single unit recording characteristics are represented by spatio-temporal from the feature vectors, querying SUR data can be implemented in two ways: from temporal feature to spatial feature, and from spatial feature to temporal feature.

5.3.3.1.1. Temporal query by trial protocols of SUR.

The fact that common trial protocols are applied across subjects enables researchers in cognitive science and neuroscience to compare features from brain signals across subjects. To compare inter-subject characteristics, the single unit recording results from one specific trial protocol are first retrieved. To query more specific features from the results with same trial protocols, users can specify a particular firing rate, time firing pattern, or frequency firing pattern, by which spatial features of single unit recordings, such as location and depth of the microelectrode, the microelectrode/neuron number as well as the basic patient information, would be retrieved as a list. If users want to explore the retrieved

data in more detail, they can access it by clicking on an item of the list. Figure 5.15 indicates a query/retrieval proposal from temporal features to spatial features.

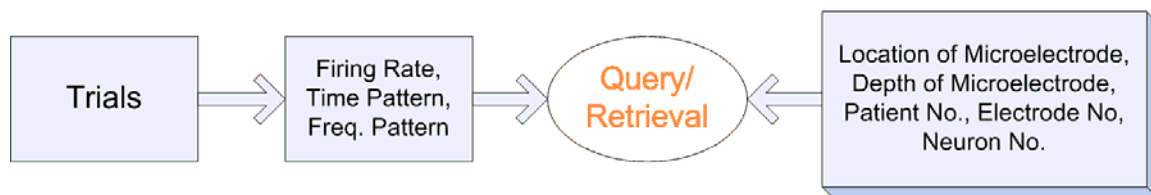


Figure 5.15 Query by trial protocols with temporal single unit recording features

5.3.3.1.2. Spatial query by trial protocols of SUR.

Shared characteristics of single unit recordings among subjects can also be queried using spatial features – that is, the location of microelectrodes. After users select one trial protocol, they can specify one location of the brain in the anatomical parcellation scheme or Brodman area. This query can retrieve temporal features, such as firing rate, firing time pattern, firing frequency pattern, with basic patient information and microelectrode/neuron number. Figure 5.16 is a diagram showing the query/retrieval route from spatial features to temporal features.

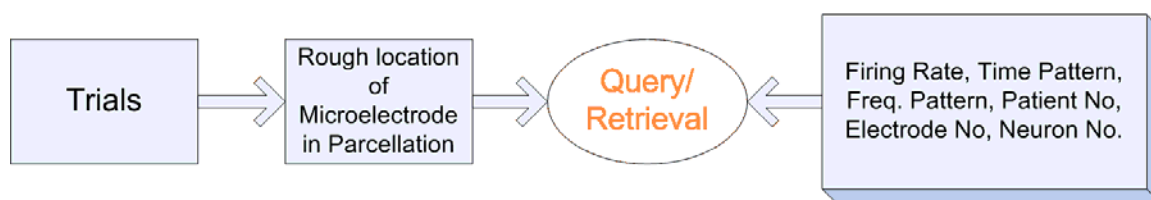


Figure 5.16 Query by trial protocols with spatial single unit recording features

5.3.3.2. Query by trial protocols of fMRI characteristics

Since fMRI activation characteristics are also represented as spatio-temporal features, query by trial protocols can be implemented as both temporal queries to spatial features, and spatial queries to temporal features.

5.3.3.2.1. Temporal query by trial protocols of fMRI.

In the fMRI query route, one trial protocol is specified following selection of the temporal characteristics of fMRI – that is, the amplitude of the hemodynamic response at the most highly activated location, and the degree of delay time of the response. By this query request, spatial features of the fMRI such as the location and the size of activations, as well as basic patient information can be retrieved. Figure 5.17 shows the search route for temporal query by trial protocols for fMRI features.

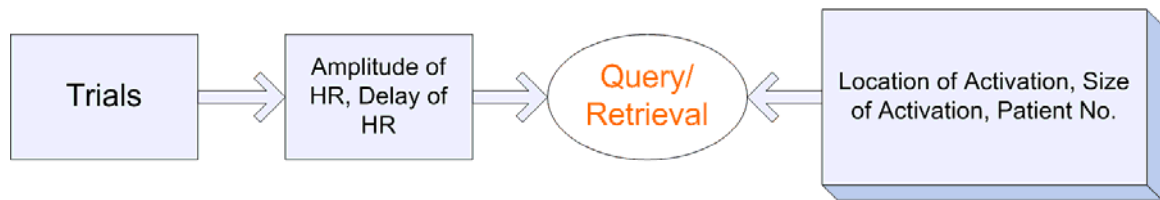


Figure 5.17 Query by trial protocols with temporal fMRI features

5.3.3.2.2. Spatial query by trial protocols of fMRI.

Since the most highly activated locations of fMRI in the brain surface are stored as indices in a content-based retrieval system, users can query activation results stimulated by one specific trial and a brain location. Following brain location selection, users can choose one trial on the anatomical parcellation scheme, by which temporal features of fMRI would be retrieved. Figure 5.18 shows a diagram of the search route for spatial query by trial protocols of fMRI.

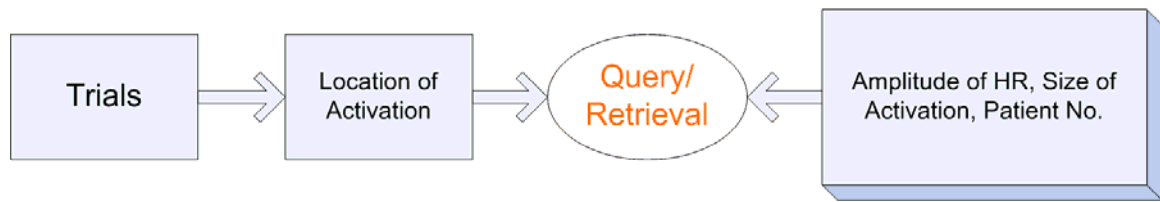


Figure 5.18 Query by trial protocols with spatial fMRI features

5.3.3.2.3. Query by trial protocols combining SUR and fMRI

When common trial protocols are applied to both fMRI and single unit recordings, the results from neuron firings of SUR and activations of fMRI can be compared to study the relationship between the two modalities. Since a shared feature of these two modalities is brain location, users can specify one location on the anatomical parcellation scheme with one requested trial protocol. Three kinds of results can be retrieved:

- (1) basic patient information with microelectrode/neuron number,
- (2) firing rate, firing time pattern, and firing frequency pattern for single unit recording data, and
- (3) amplitude, size and degree of delay time of hemodynamic responses

Figure 5.19 shows a search idea about query by trial protocols combined with fMRI and single unit recording characteristics.

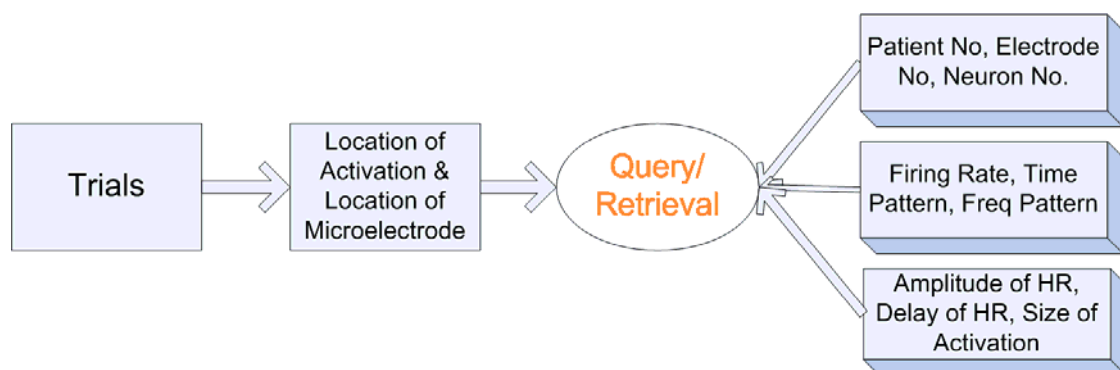


Figure 5.19 Query by trial protocols combining with fMRI and single unit recording characteristics

5.3.3.3. Graphical user interface for query by trial protocol

In the graphical user interfaces, when users select the second search route ‘Query by trial protocols’, they choose a method from ‘SUR’, ‘fMRI’, and ‘SUR-fMRI’. The method they choose determines the appropriate paradigm for the trial protocols to be searched. Subsequent menus are then displayed according to the method the user has selected. Figure 5.20 is a screen shot of the initial screen of query by trial protocols.

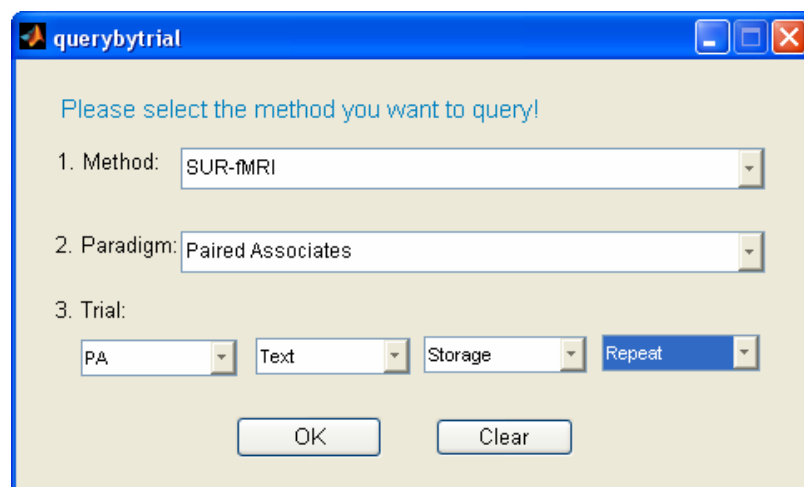


Figure 5.20 A screen shot of the initial screen of query by trial protocols

If ‘fMRI query’ is selected as a method for query by trial protocols, a location in the brain must be specified on a canonical brain image. To specify a brain location, the anatomical parcellation scheme pops up as in Figure 5.21, and the users can then choose a parcel by clicking with the mouse. To refine the query, the activation level and delay of hemodynamic response on the most highly activated voxel in the specified location are also selected as shown in Figure 5.22.

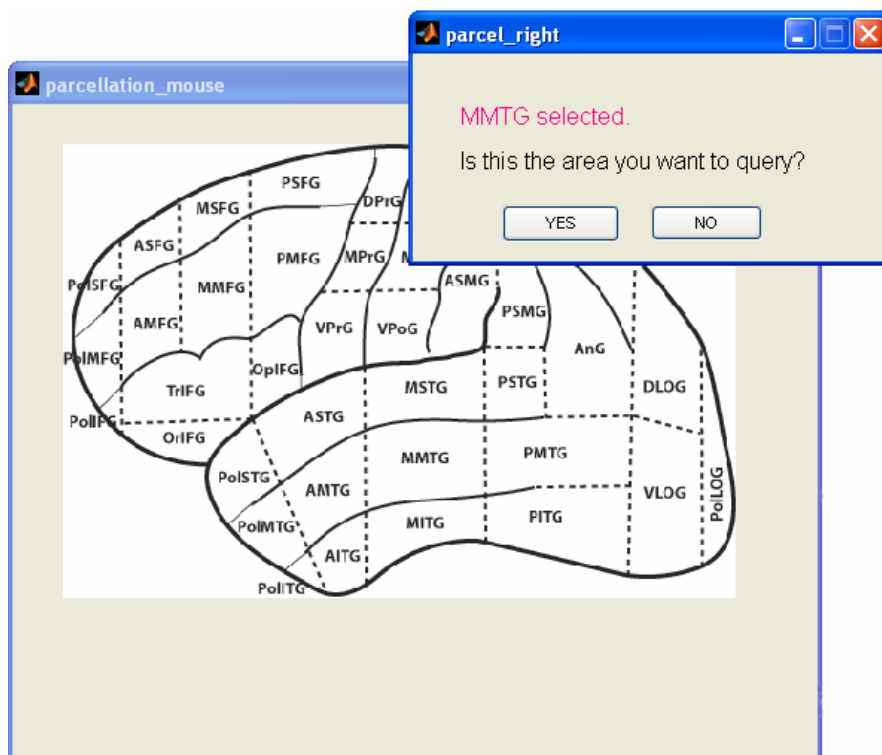


Figure 5.21 A screen shot to select a brain location in the anatomical brain parcellation scheme

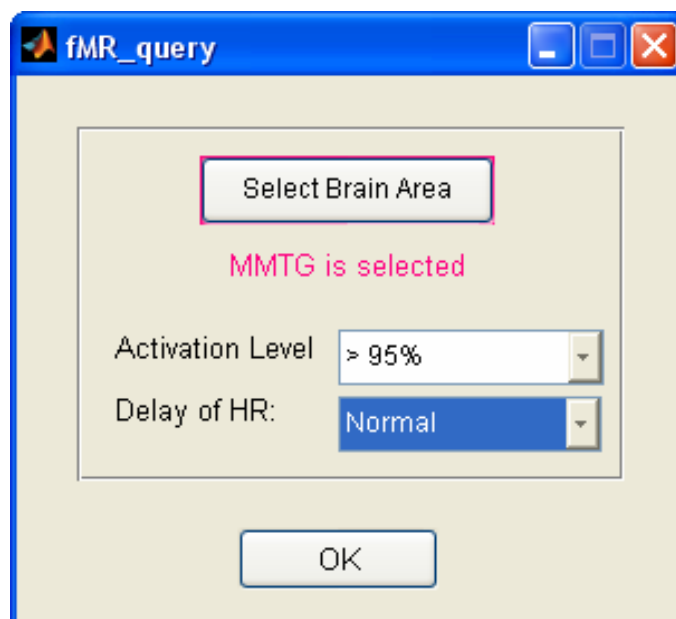
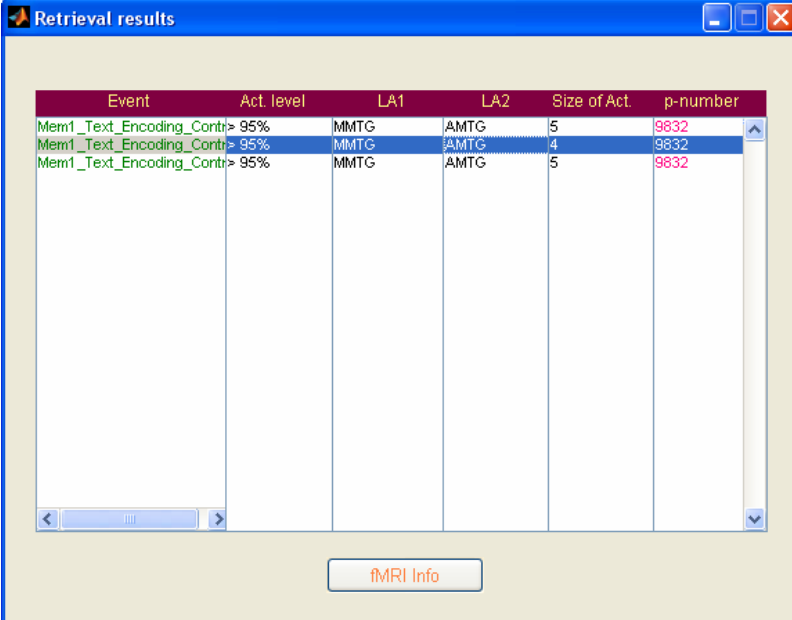


Figure 5.22 A screen shot to select activation level and delay of hemodynamic responses.

After selecting the fMRI indices for the query, matching data is retrieved by patient number and by the second most highly activated location, from which users may pick an item they want to see in more detail, as in Figure 5.23.



Event	Act. level	LA1	LA2	Size of Act.	p-number
Mem1_Text_Encoding_Contr> 95%		MMTG	AMTG	5	9832
Mem1_Text_Encoding_Contr> 95%		MMTG	AMTG	4	9832
Mem1_Text_Encoding_Contr> 95%		MMTG	AMTG	5	9832

Figure 5.23 A screenshot to display a list of fMRI results for a specific query

After an item on the fMRI list is selected, the retrieved results of trial protocol information, patient number, and location and size of fMRI activations with 3-D surface mapping are displayed, as shown in Figure 5.24.



Figure 5.24 A screenshot to display fMRI activation results

If 'SUR' menu is selected as a method for 'Query by trial protocols' search route, a list similar to Figure 5.25 is arranged and displayed by the requested trial protocols. When an item is selected, the results of firing patterns and firing rate are retrieved as in Figure 5.26. Furthermore, if 'SUR-fMRI' menu is selected as a method for 'Query by trial protocols' search route, both fMRI and single unit recording indices are to be specified, as shown in Figure 5.25.

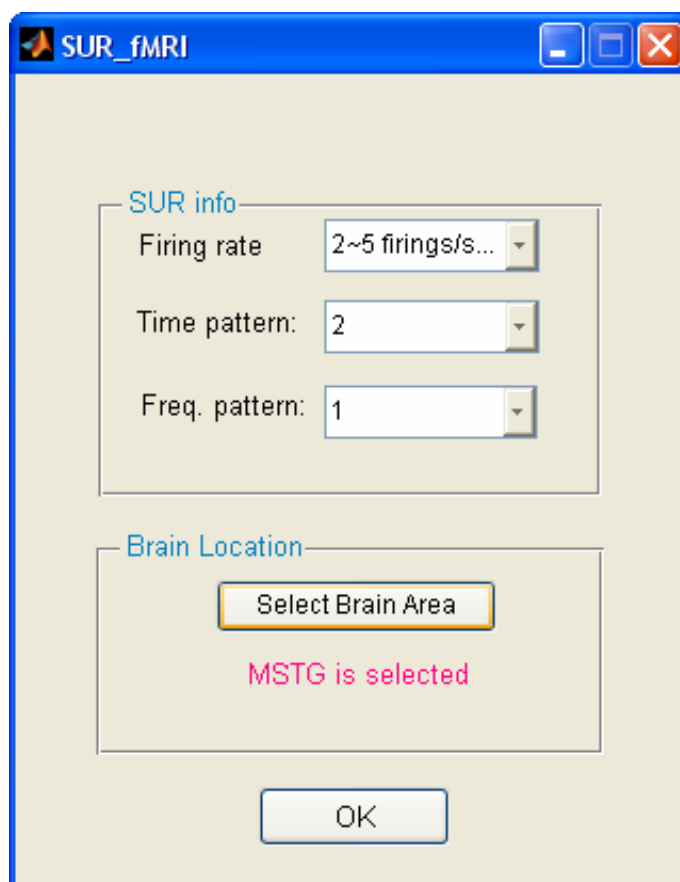


Figure 5.25 A screenshot to select firing rate and time patterns for single unit recording, and a brain location for fMRI

The retrieved data by the 'Query by trial protocols' search route and the combination of SUR and fMRI contains both neuron firing patterns and the firing rate of the single unit recording. Hemodynamic response vectors of fMRI are also displayed in order to compare and analyze the two modalities, as shown in Figure 5.26. The result also contains basic patient information and the location on the canonical brain image. This comparison is very useful for further investigation of relationships between firing patterns of single unit recording and hemodynamic responses of fMRI.

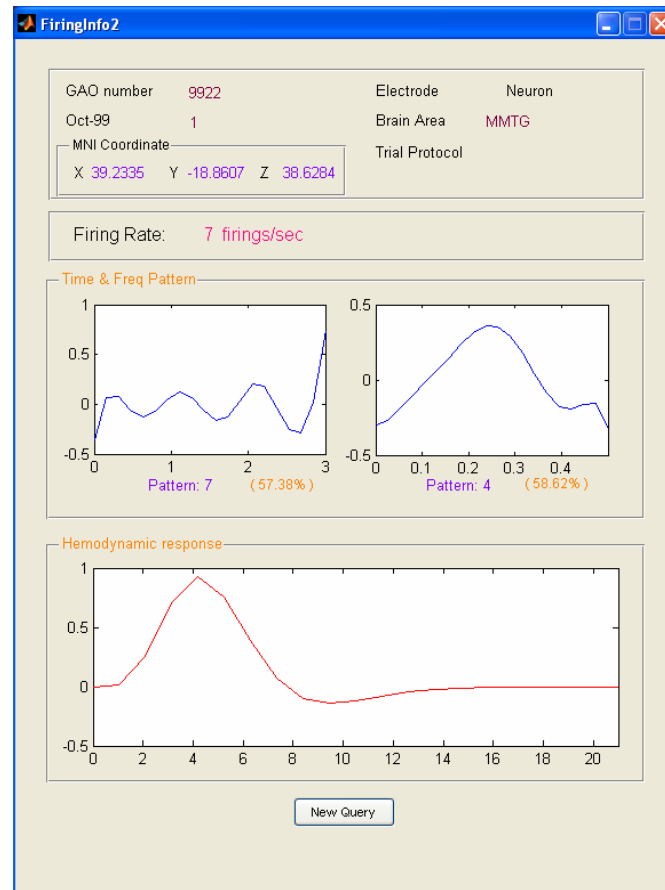


Figure 5.26 A screenshot to show neuronal firing patterns with hemodynamic responses.

5.3.4. Query by firing patterns and/or fMRI activations

While the query by trial protocols is used to find the relationships among brain signals across subjects for some specific stimuli, query by firing patterns and/or fMRI activations finds which trial protocols stimulate similar firing patterns or activations.

5.3.4.1. Query by firing patterns of SUR

To determine which trial protocols stimulate a specific firing pattern, both temporal and spatial queries can be posed, combined with specific time and frequency patterns.

5.3.4.1.1. Temporal query by firing patterns

With specific neuron time and frequency firing patterns, users can query which trial protocol causes those firings in which patients and which microelectrode/neurons. Even though neuron spikes have similar firing patterns, the query results can be refined by the average firing rate. This characteristic is one of the most important features of single unit recordings. After the primary and secondary firing patterns are selected, the average firing rate is also chosen as a numerical range to query trial protocols and the patient information. Figure 5.27 shows query by firing pattern with temporal features of the single unit recordings.

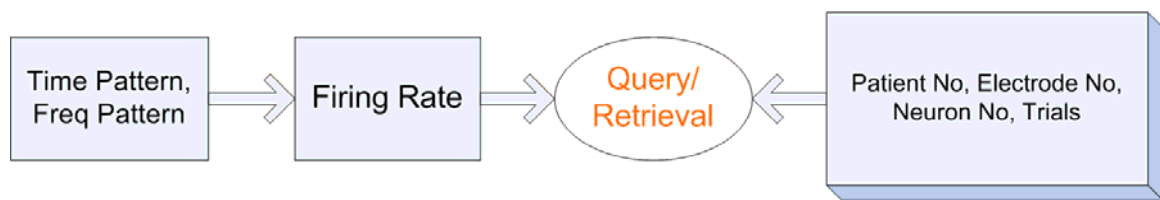


Figure 5.27 Query by firing pattern with temporal SUR features

5.3.4.1.2. Spatial query by firing patterns

When users want to know which firing patterns are caused by what kind of trial protocols in a particular portion of the brain, the data can be queried spatially. Searching a time pattern and a frequency pattern with the corresponding frequencies in a specific brain location can be carried out by clicking one portion on the anatomical parcellation scheme or Brodman area. With this query, the basic patient information and microelectrode/neuron number with matching trial protocols are retrieved. Figure 5.28 shows the search route for spatial query by firing patterns.

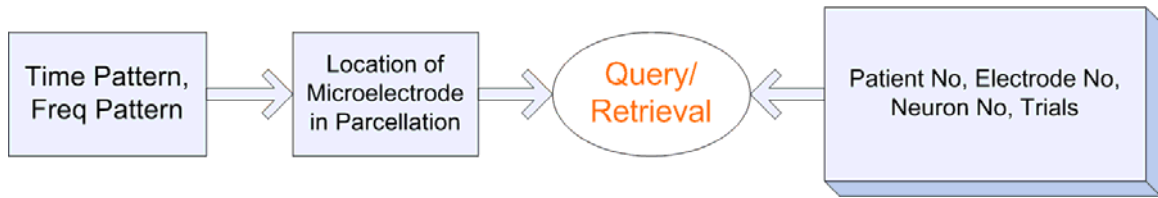


Figure 5.28 Query by firing pattern with spatial SUR features

5.3.4.2. Query by fMRI activations

Using the results of fMRI activations only, the basic patient information and protocol trials can be queried. With this query, users can find which activations on a brain location are brought about by which trial protocols on which patients. Users can specify a brain location with activations greater than a given size to query the data. Figure 5.29 is a diagram showing query by fMRI activation.

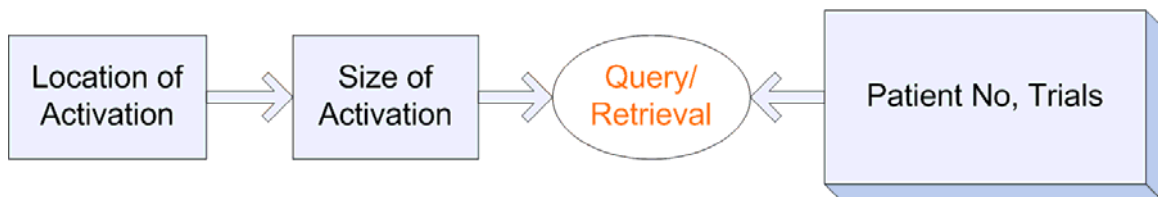


Figure 5.29 Query by fMRI activation

5.3.4.3. Query by the common features in both SUR and fMRI

Since the location of a microelectrode/neuron and the position of fMRI activation are the same in both SUR and fMRI activations, users can query common features for these locations. After choosing a location on a canonical brain image, users can specify the firing time pattern and the frequency pattern as single unit recording features and size of activation as an fMRI feature to query common characteristics, such as the basic patient information and trial protocols. Figure 5.30 shows a query and retrieval path using a brain location shared by both fMRI and SUR.

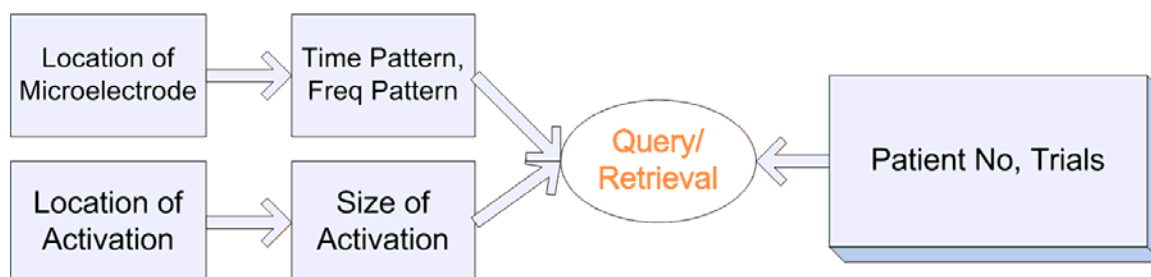


Figure 5.30 Query by brain location shared by both fMRI and SUR

5.3.4.4. Graphical user interface for query by firing patterns and/or fMRI activations

If query by firing patterns and/or fMRI activations menu is selected as a search route, a list containing queried firing patterns and/or fMRI activations from the database is displayed as Figure 5.23 among which users can select an item to show the retrieved result as shown in Figure 5.26. By this query, the relationship of time firing patterns and hemodynamic responses can be observed.

Using this query system, users in the brain-related fields, such as neuroscience or cognitive science, can study which relationships exist between action potential of single neuron and activations of fMRI at a location for specific trial protocol.

5.3.5. Bidirectional query by SUR with fMRI and by fMRI with SUR.

Since one of the most important aspects of this content-based retrieval system of the functional human brain is to discover the relationships between fMRI activations and firing patterns of action potentials, a combined search route of the two modalities is also provided. A shared characteristic of fMRI and SUR is the brain location in a canonical brain image, which is used as a cross-reference. With the information from single unit recordings such as the location of a microelectrode, fMRI activations near that microelectrode can be identified and

trial protocols, amplitudes and sizes of hemodynamic responses, response vectors, and basic patient information can be retrieved. If users choose the location of a microelectrode on the anatomical parcellation scheme or the Brodman area that they want to query, the distances from the microelectrode to the location of the fMRI activations are computed to make a list of the closest activations. Figure 5.31 shows the search route to query by information of single unit recording to fMRI activation features.

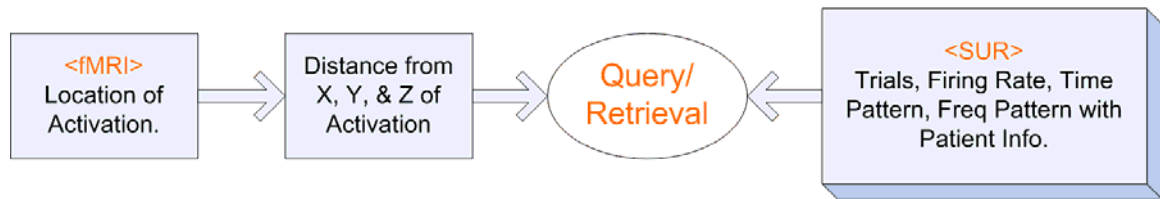


Figure 5.31 Query by information of single unit recording for fMRI activation features.

On the other hand, with fMRI activation such as location of activation, the single unit recording information near the location of the fMRI activation can be retrieved, i.e. trial protocols, time firing patterns, frequency firing patterns, and basic patient information. Figure 5.32 is a diagram showing the search route to query by fMRI information to single unit recording features.

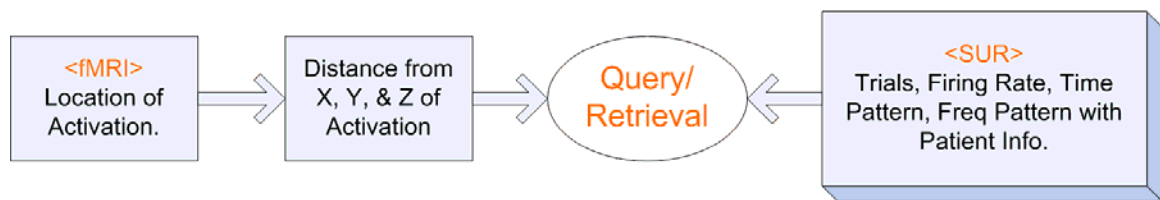


Figure 5.32 Query by fMRI information with brain location for single unit recording features

The distances from fMRI activations to the microelectrode of a single unit recording are calculated by the Euclidean metric between two points on a canonical brain image. However, the retrieved results are listed in the order of

closest distances, from which users can query more information by clicking an item.

5.4. Discussion

To evaluate this system, three separate datasets mentioned in the section 5.3 are loaded. The accuracy of the prototype of the content-based retrieval system implemented in this research depends on the feature extraction and indexing. If the features of fMRI and SUR can be extracted exactly, search results will be accurate. To reduce indexing errors, probabilistic approaches, such as primary and secondary pattern templates, are used. The response time of the retrieval system is based on text-based retrieval time and multimedia data loading time.

Chapter 6

CONCLUSIONS

In this dissertation, a methodology for classification of functional brain data and query algorithm to build a multimedia retrieval system including both fMRI and single unit recording of neurons acquired during neurosurgery has been proposed, and a prototype system for multimedia retrieval of such data has been designed and implemented. This study made data from multi-modalities be linked by unified features and the retrieval system can help neuroscientists store and retrieve their data and do post-experiment analysis. The main contributions of the work are as follow:

1. a new algorithm for detecting activations in functional magnetic resonance imaging
2. a new method for neuron spike sorting
3. a procedure to characterize firing patterns of neuron spikes from the human brain, in both temporal domain and the frequency domain, and
4. construction of data and index structures, and a prototype retrieval system.

6.1. Future directions of research

To understand the functions of brain in much more detail, various studies of functional brain images, such as positron emission tomography (PET), electroencephalogram (EEG), and/or Electrocortical (ECoG) activities as well as fMRI and SUR, are to be more researched and collaborated.

The first issue we need to address in the future to achieve more accurate results of functional brain signal is to improve and automate fMRI feature extraction. The second issue is to upgrade and automate brain image registration as well as positioning for fMRI and SUR.

The content-based retrieval system will support multiple types of queries and permits visualization of the results of those queries in a way that promotes further investigation of the relationship among the firing patterns of single neurons and the fMRI activations. The prototype implemented in this research will be carried out in feasible database, for which we will collaborate with the Structural Informatics Group, University of Washington. Figure 6.1 shows a diagram to show the relationship of each index and query idea to be implemented in the real database.

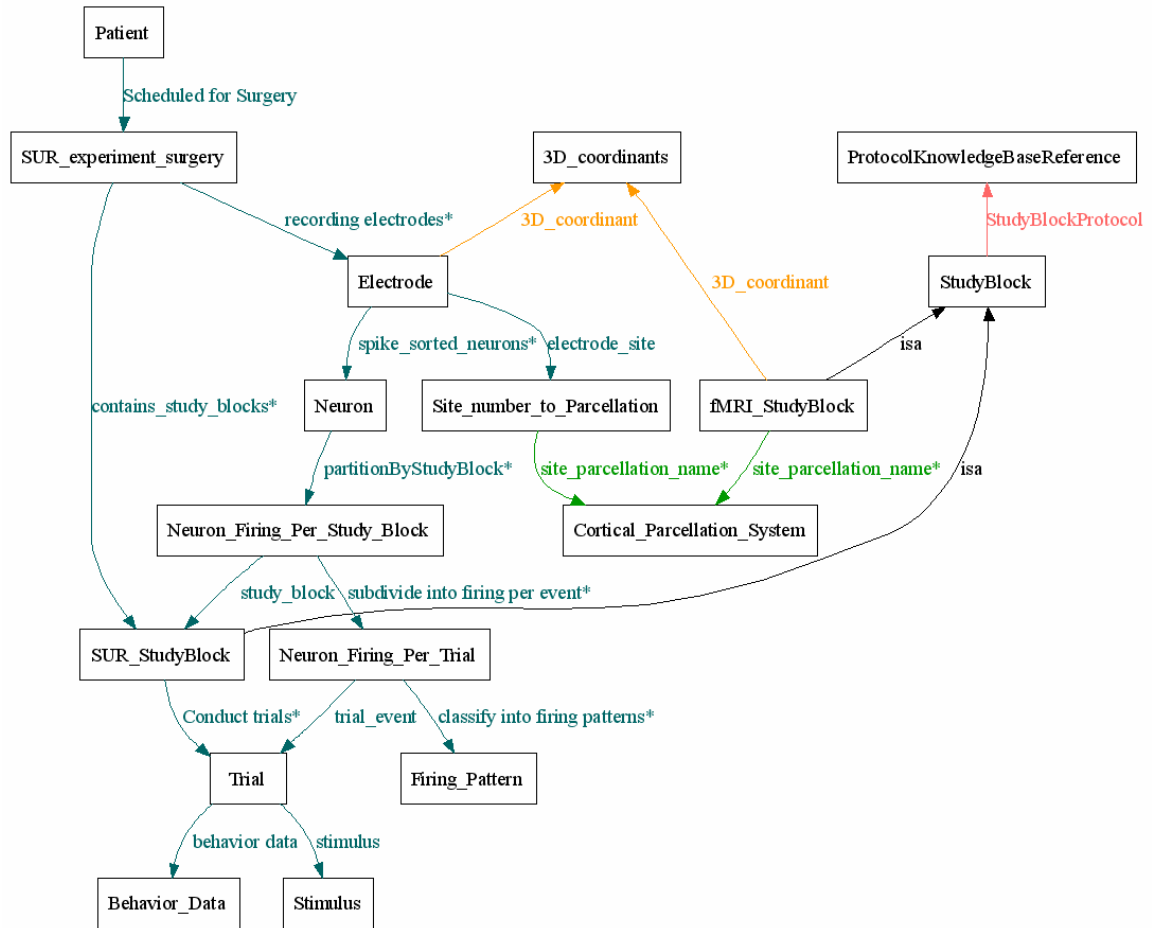


Figure 6.1 A diagram to show the relationship of each index and query idea.

BIBLIOGRAPHY

- [1] J. F. Brinkley, C. Rosse, "Imaging and the Human Brain Project: a review", *Methods of Information in Medicine*, v 41, n 4, 2002, p 245-60
- [2] Hansang Cho, G.A. Ojemann, David Corina, and Linda Shapiro, "Detection of Neural Activity in Event-related fMRI using Wavelet and Dynamic Time Warping", *Applications of Digital Image Processing XXVI, Proceedings of SPIE*, vol. 5203, 2003, pp. 638-647

- [3] Hansang Cho, D. Corina, G. A. Ojemann, J. Schoenfield, Leona Zamora, and Linda Shapiro, "A new neuron spike sorting method using maximal overlap discrete wavelet transform and rotated principal component analysis", *Engineering in Medicine and Biology Society, 2003. Proceedings of the 25th Annual International Conference of the IEEE*, Vol.3, pp. 2921-2924

- [4] A. M. Dale and R. L. Buckner, "Selective averaging of rapidly presented individual trials using fMRI," *Human Brain Mapping*, vol. 5, pp. 1~12, 1997

- [5] B. Rosen, T.L. Buckner, and A. M. Dale, "Event-related fMRI: Past, present and future," *PNAS*, vol. 95, 1998 pp.773-780

- [6] V. Solo, P.Purdon, R. Weisskoff, and E. Brown, "A signal estimation approach to functional MRI," *IEEE transactions on medical imaging*, vol. 20, No. 1, 2001, pp. 26~35

- [7] Shin-Chung Ngan, Williams F. Aufermann, Shananu Sarkar, and Xiaoping Hu, "Activation detection in event-related fMRI data based on spatio-temporal properties," *Magnetic Resonance Imaging*, vol. 19, 2001, pp. 1149-1158

- [8] Ramus M. Birn, Robert W. Cox, and Peter A. Bandettini, "Detection versus Estimation in event-related fMRI: Choosing the optimal stimulus timing", *NeuroImage*, vol.15, 2002, pp.252-264

- [9] Mark Jenkinson and Stephen Smith, "The Role of Registration in Functional Magnetic Resonance Imaging," *Medical Image Registration*, CRC, 2001, pp. 183-198

- [10] Ola Friman, Magnus Borga, Peter Lundberg, and Hans Knutsson, "Detection of Neural Activity in fMRI using maximum correlation modeling," *NeuroImage*, vol. 15, 2002, pp. 386-395

- [11] Oliver Josephs, Robert Turner, and Karl Friston, "Event-related fMRI", *Human Brain Mapping*, vol.5, 1997, pp.243-248.

- [12] Anders M. Dale, "Optimal Experimental Design for event-related fMRI", *Human Brain Mapping*, vol.8, 1999, pp.109-114

- [13] Martin J. McKeown, et al. "Analysis of fMRI data by blind separation into independent spatial components", *Human Brain Mapping*, vol.6, 1998, pp. 160-188

- [14] A. H. Andersen, D. M. Gash, and M. J. Avison, "Principal component analysis of the dynamic response measured by fMRI: A generalized linear system framework," *Magn. Reson. Imag.*, vol. 17, no. 6, pp. 795-815, 1999

- [15] M. J. Fadili, S. Ruan, D. Bloyet, and B. Mazoyer, "Unsupervised fuzzy clustering analysis of fMRI series," in *Proc. 20th Annu. Int. Conf. IEEE Engineering Medicine Biology*, vol. 20, 1998, pp. 696-699

- [16] Andrew F. Laine, "Wavelets in temporal and spatial processing of biomedical images", *Annual review biomedical engineering*, vol.2, 2000, pp. 511-550

- [17] Donald B. Percival, and Andrew T. Walden, Wavelet methods for time series analysis, *Campridge*, 2000, ch. 5, pp. 159-179

- [18] Woon-Young So, and Dong-Seok Jeong, "A study on the postprocessing of functional MRI using overcomplete wavelet transform", *IEEE Tencon*, 1999, pp. 1174-1177

- [19] Ben Gold and Nelson Morgan, "Speech and audio signal processing, processing and perception of speech and music," *John Wiley & Sons*, 1999, pp.327-333

- [20] B. Huang and W. Kinsner, "ECG frame classification using dynamic time warping", *Proceedings of the 2002 IEEE Canadian conference on Electrical and computer engineering*, 2002, pp. 1105-1110

- [21] Sergios Theodoridis and Konstantinos Koutroumbas, "Pattern Recognition", *Academic Press*, 1998, pp.284-300

- [22] David P. Corina; Todd L. Richards; Sandra Serafini; Anne L. Richards; Keith Steury; Robert D. Abbott; Denise R. Echelard; Kenneth R. Maravilla, and Virginia W. Berninger, "fMRI auditory language differences between dyslexic and able reading children", *Neuroreport* 2001 May 8;12(6): pp. 1195-201

- [23] Michael S Lewicki, "A review of methods for spike sorting: the detection and classification of neural action potentials", *Network*, Nov;9(4). pp. R53-78, 1998

- [24] J. P. Stitt, R. P. Gaumond, J. L. Frazier, and F. E. Hanson, "A comparison of neural spike classification techniques", in *Proc. 19th international conf. IEEE/EMBS* 1997, Chicago, IL, pp. 1092-1094

- [25] M. Barlow, S. Nigam, and E. H. Berbery, "ENSO, pacific decadal variability, and U.S. summertime precipitation, drought, and stream flow", *American meteorological society*, vol. 14, pp. 2105-2128, 2001
- [26] Marquardt, D., "An Algorithm for Least-Squares Estimation of Nonlinear Parameters," *SIAM J. Appl. Math.* Vol. 11, pp 431-441, 1963
- [27] Donald B. Percival and Andrew T. Walden, "Spectral Analysis for Physical Applications", *Cambridge University Press*, 1993, pp. 331-347
- [28] Press W., Flannery B., Teukolsky S., and Vetterling W., "Numerical recipes in C", *Cambridge University Press*, 1988. pp. 542-7
- [29] R. F Martin, J. F. Brinkley, X. Hertenberg, A. V. Poliakov, D. P. Corina, and G. A. Ojemann, "Anatomical Parcellation of Cortical Language Sites", *Proceedings, MedInfo 2004*, pages 1742, San Francisco, CA
- [30] D. L. Collin, P. Neelin, T. M. Peters, and A. C. Evans, "Automatic 3-D intersubject registration of MR volumetric data in standardized Talairach space", *Journal of Computer Assisted Tomograph*, 1994, 18(2): pp. 192-205.
- [31] A.V. Poliakov, E. Albright, K.P. Hinshaw, D.P. Corina, R.F. Martin, and Brinkley, J.F., "Server-based Approach to Web Visualization of Integrated Three-dimensional Brain Imaging Data". *Journal of the American Medical Informatics Association*, 2005 Mar-Apr, 12(2), pp.140-151.
- [32] A.V. Poliakov, K.P. Hinshaw, C. Rosse, and J. F. Brinkley, "Integration and visualization of multimodality brain data for language mapping.", *Proc AMIA Symposium*, 1999, pp. 349-53.

VITA

Hansang Cho obtained the B.S. degree in Electronics Engineering from the Kwangwoon University in Seoul, Korea in 1994. He received the M.S. and Ph.D. in Electrical Engineering from the University of Washington at Seattle in 1998 and 2005. He worked for the Samsung Electronics Co. in Kyungki-do, Korea and the Spencer Technologies in Seattle, WA in 1994 and 1999. He joined the Cognitive Neuropsychology Laboratory at the University of Washington in 1999. His research interest includes pattern classification, medical signal analysis, and content-based retrieval system. At present he is an algorithm engineer at the SVision LLC at Seattle, WA.